molecular pharmaceutics

Article

Cite This: Mol. Pharmaceutics 2019, 16, 3237−3252

pubs.acs.org/molecularpharmaceutics

Hydrophilic Small Molecules That Harness Transthyretin To Enhance the Safety and Efficacy of Targeted Chemotherapeutic Agents

Arindom Pal,[†,§] Wabel Albusairi,[†,§] Fang Liu,[†] Md Tariqul Haque Tuhin,[†] Mark Miller,[†] Dengpan Liang,[†] Hyun Joo,[†] Toufiq Ul Amin,[†] Elizabeth A. Wilson,[‡] Jesika S. Faridi,[‡] Miki Park,[†] and Mamoun M. Alhamadsheh*[,†]

[†]Department of Pharmaceutics & Medicinal Chemistry, Thomas J. Long School of Pharmacy & Health Sciences and [‡]Department of Physiology and Pharmacology, University of the Pacific, Stockton, California 95211, United States

Supporting Information

ABSTRACT: The hydrophobicity of many chemotherapeutic agents usually results in their nonselective passive distribution into healthy cells and organs causing collateral toxicity. Ligand-targeted drugs (LTDs) are a promising class of targeted anticancer agents. The hydrophilicity of the targeting ligands in LTDs limits its nonselective passive tissue distribution and toxicity to healthy cells. In addition, the small size of LTDs allows for better tumor penetration, especially in the case of solid tumors. However, the short circulation half-life of LTDs, due to their hydrophilicity and small size, remains a significant challenge for achieving their full therapeutic potential. Therefore, extending the circulation half-life of targeted chemotherapeutic agents while maintaining their hydrophilicity and small size will represent a significant advance toward effective and safe cancer treatment. Here, we present a new approach for enhancing the safety and efficacy of targeted chemotherapeutic agents. By endowing hydrophobic chemotherapeutic agents with a targeting moiety and a hydrophilic small molecule that binds reversibly to the serum protein transthyretin, we generated small hydrophilic drug conjugates that displayed enhanced circulation half-life in rodents and selectivity to cancer cells. To the best of our knowledge, this is the first demonstration of a successful approach that maintains the small size and hydrophilicity of targeted anticancer agents containing hydrophobic payloads while at the same time extending their circulation half-life. This was demonstrated by the superior in vivo efficacy and lower toxicity of our conjugates in xenograft mouse models of metastatic prostate cancer.

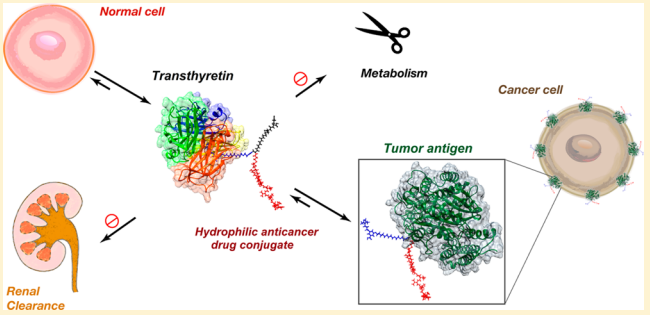

KEYWORDS: *hydrophilic transthyretin ligands, half-life extension, targeted chemotherapeutic agents, prostate cancer, PSMA ligands*

INTRODUCTION

Most chemotherapeutic agents are designed to interfere with processes inside a tumor cell. These cytotoxic drugs should be hydrophobic enough to diffuse across cell membranes and reach their intracellular targets. However, the hydrophobicity of these drugs will usually result in their nonselective passive distribution into healthy cells and organs resulting in collateral toxicity. Therefore, strategies that minimize the toxicity of these cytotoxic agents toward healthy cells while maintaining their potency on tumor cells are highly desirable. One attractive strategy for achieving the required therapeutic potency with minimal toxicity is through targeted cancer therapy.[1] Antibody−drug conjugates (ADCs) represent a promising approach for cancer therapy that involves conjugation of the cytotoxic agent to antibodies targeted to specific tumor antigens. While the large size of ADCs (size ∼150 kDa) limits the nonselective distribution of the cytotoxic agent into healthy cells and tissues, it also reduces their rate of diffusion and extent of penetration into solid tumor tissues. Therefore, the majority of approved ADCs and the ones in clinical trials are used in hematologic cancers. The limited number of ADCs used in the treatment of solid tumors led many to explore alternative, smaller-format drug conjugates with better tumor penetrating properties.[2−4]

Ligand-targeted drugs (LTDs) that employ low-molecular weight hydrophilic small molecules or peptides as targeting moieties (e.g., vintafolide, etarfolatide, and ^{177}Lu-PSMA-617) are a promising new class of targeted cancer therapeutics.[1,2] The small size of LTDs (typically ∼1 to 5 kDa) allows for better tumor penetration, especially in the case of solid tumors. In addition, the hydrophilicity of the targeting ligand increases the overall hydrophilicity of the hydrophobic cytotoxic payload in the LTD, which limits its nonselective passive tissue distribution and toxicity to healthy cells. On the other hand, hydrophilic small molecules are readily cleared through the

Received: April 22, 2019
Revised: May 22, 2019
Accepted: May 28, 2019
Published: May 28, 2019

DOI: 10.1021/acs.molpharmaceut.9b00432
Mol. Pharmaceutics 2019, 16, 3237−3252

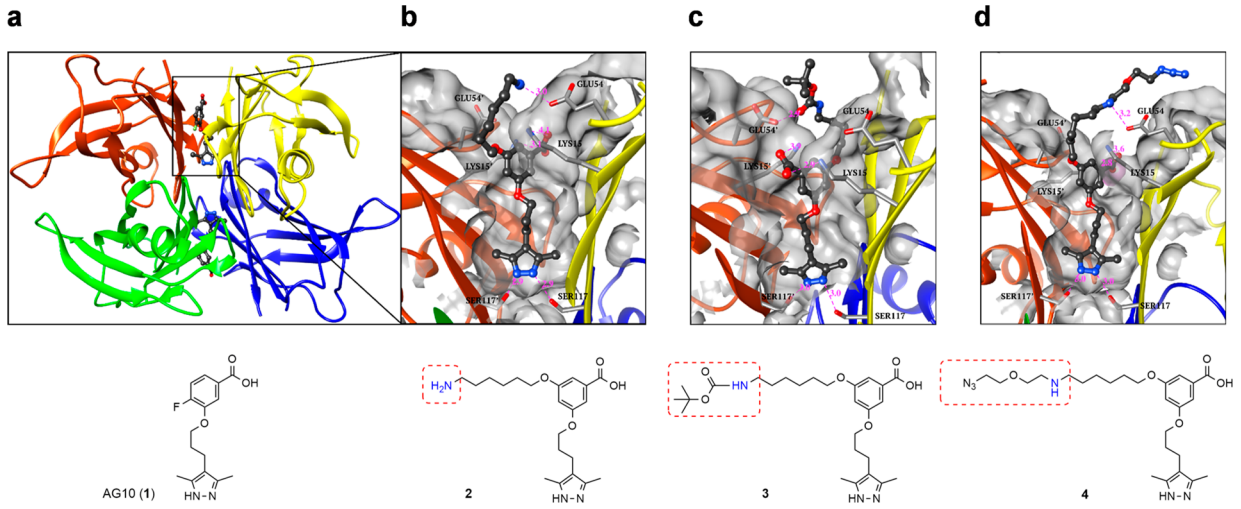

Figure 1. Crystal structure of TTR bound to AG10 and modeled hydrophilic TTR ligands. (a) Crystal structure of homotetrameric TTR bound to AG10, with monomers colored individually (PDB ID: 4HIQ).[10] Two AG10 molecules are bound in the two thyroxine (T_4) binding site in TTR. (b–d) Close-up views of modeled TTR ligand **2**, **3**, and **4** bound in one of the two TTR T_4 pockets. The putative salt bridges between the amine group of TTR ligands **2** and **4** with Glu54/Glu54′ of TTR are shown as dashed lines and the distances are given in Å.

kidneys within 30 min of injection (size cutoff for molecules to be cleared through glomerular filtration is ∼30 kDa).[5] The short in vivo half-life ($t_{1/2}$) of LTDs (e.g., $t_{1/2}$ for vintafolide and etarfolatide is ∼25 min) reduces their exposure to receptor-expressing target tissues which prevents optimal tumor uptake.[2] Therefore, dose-limiting toxicity is observed due to the need for high doses and frequent administration.[6]

Conjugation of polyethylene glycol (PEG) polymers (∼20 to 40 kDa) to LTDs has extended their in vivo $t_{1/2}$. However, the large size of PEG impedes the penetration of these LTDs deep in the solid tumor tissue, with most of the conjugates concentrated near the perfusing blood vessels.[3] Conjugation of hydrophobic small-molecule albumin binders to radioimaging LTDs, containing hydrophilic DOTA chelators as the payload, has resulted in small conjugates with extended circulation time and higher tumor uptake.[7,8] Unfortunately, the albumin binding approach has not been successfully used with LTDs containing cytotoxic therapeutic payloads, where the warheads are typically ultrapotent hydrophobic small molecules (e.g., auristatins and maytansinoids). In this case, conjugation to the lipophilic albumin binders will increase the overall hydrophobicity of LTDs, which could make them prone to aggregation, micelle formation, or nonspecific diffusion and adsorption to off-target cells.[2] Therefore, extending the in vivo $t_{1/2}$ of LTDs while maintaining their hydrophilicity and smaller size, which are crucial for selectivity and better tumor penetration, will represent a significant advance toward effective and safe cancer treatment.

Our group has previously repurposed a derivative of the potent transthyretin (TTR; a 56 kDa serum protein present at ∼5 μM concentration, Figure 1a) stabilizer, AG10 (**1**) for a $t_{1/2}$ extension approach for peptides.[9,10] AG10 is currently in Phase III clinical trials for TTR cardiac amyloidosis. We developed linker-modified AG10 molecules that were conjugated to hydrophilic peptides (e.g., GnRH; Log P −3.6), which resulted in enhanced in vivo $t_{1/2}$ of the peptide conjugates.[9] We hypothesized that such an approach could be utilized to enhance the safety and efficacy of targeted anticancer agents containing hydrophobic payloads. However, the linker we used in these first generation TTR binders was a lipophilic alkyl linker. Therefore, conjugation of these TTR binders to a hydrophobic cytotoxic agent such as monomethyl auristatin E (MMAE; Log P + 3.1) would not result in conjugates with an overall hydrophilic character. We anticipate these conjugates to have nonselective passive diffusion into healthy cells. We hypothesize that by increasing the hydrophilicity of the TTR ligands we could balance the effect of the hydrophobic MMAE in the conjugates. This would confer overall hydrophilicity on cytotoxic conjugates, limiting their passive diffusion into healthy cells.

Herein, we developed a second generation hydrophilic TTR ligands and demonstrated that they can be utilized in a targeted drug delivery system that enhances the safety and efficacy of targeted anticancer agents containing hydrophobic cytotoxic agents. We show that conjugation of the new TTR ligands to LTDs, targeting prostate cancer (PCa) cells, maintains the overall hydrophilicity of the conjugates. Because of their hydrophilicity, and ability to bind to TTR, our conjugates displayed reduced toxicity toward healthy cells (by limiting nonselective passive tissue distribution). In addition, the TTR ligands also allow these conjugates to bind reversibly to circulating endogenous TTR, which increased their in vivo $t_{1/2}$ in rats and mice. Our approach has the unique advantage of maintaining the overall hydrophilicity and small size of these conjugates, while at the same time enhancing their circulation $t_{1/2}$. This was translated into superior in vivo efficacy of our conjugates, compared to typical LTDs, in mouse xenograft tumor models of metastatic PCa.

EXPERIMENTAL SECTION

Materials and Reagents. Prealbumin from human plasma (human TTR) was purchased from Sigma (Sigma: #P1742). Amplex Red Glutamic Acid/Glutamate Oxidase Assay Kit (Invitrogen, Fisher Scientific; Molecular Probes, A12221). N-Acetylaspartylglutamate (NAAG; MP Biomedicals, ICN15303625), rhPSMA (R&D Research, 4234ZN010). rhPSMA (20 μM in reaction buffer; R&D Research, 4234ZN010), PMPA obtained from Tocris (cat # 13−801−0). Human prostate carcinoma cell lines LNCaP (PSMA+) (ATCC CRL-1740) and DU145 (PSMA−) (ATCC HTB81)

DOI: 10.1021/acs.molpharmaceut.9b00432
Mol. Pharmaceutics 2019, 16, 3237−3252

Scheme 1. Synthesis of BFM1 and TFM1: TTR Ligand 2 (Blue), PSMA Ligand (Black), Payload (Cy7 in Red), and Linker System (Magenta)

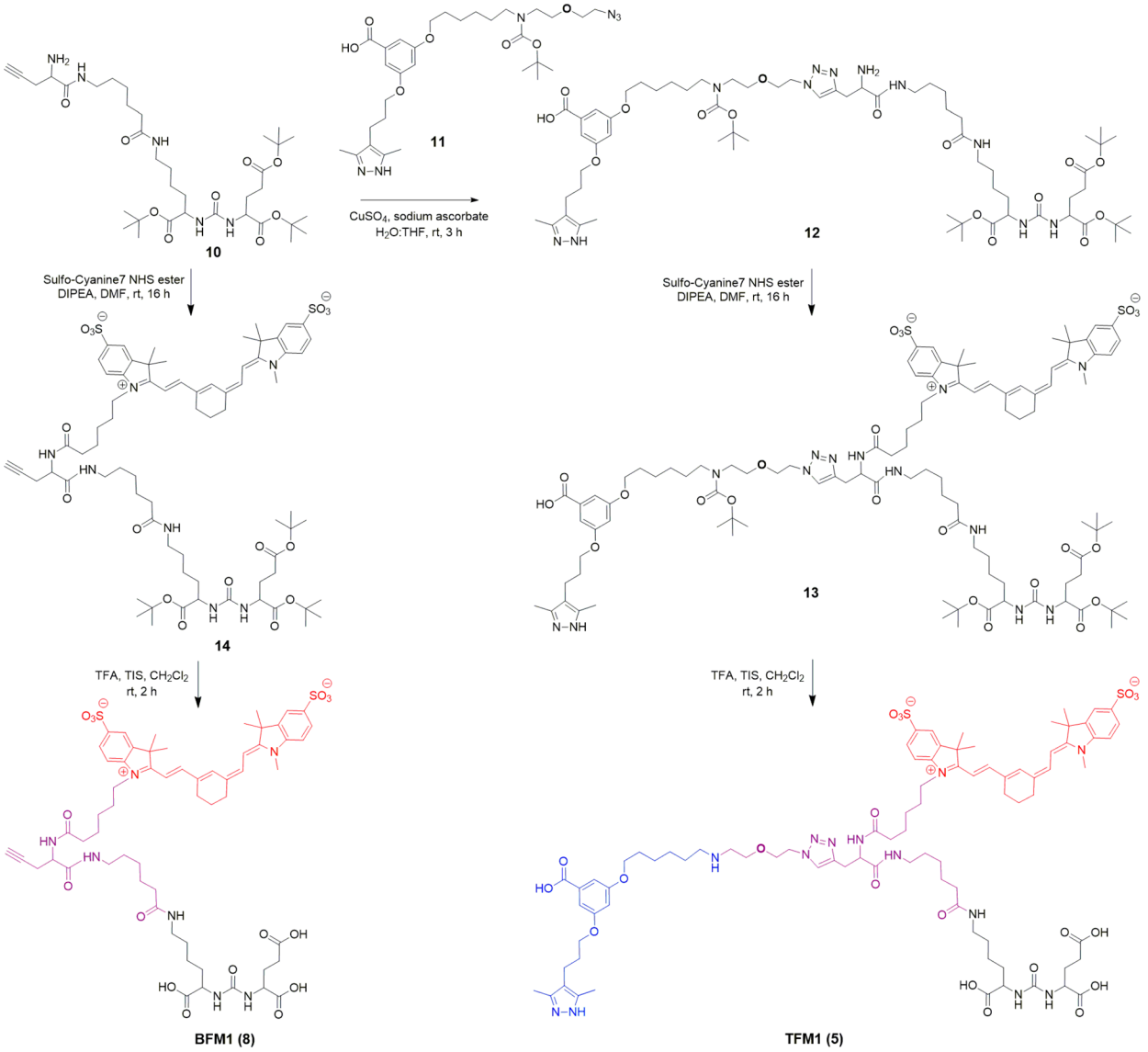

cell lines were obtained from American Type Culture Collection (ATCC), Manassas, USA. Cathepsin B from human liver was purchased from Calbiochem, EMD Millipore Corp (# 219362−50UG). Rabbit anti-RBP4 antibody was purchased form Abcam (#ab154914). IRdye800 donkey antirabbit secondary antibody was purchased from LI-COR Biosciences (#926−32213).

Chemical Synthesis and HPLC Purity Analysis. The synthesis of TFM1−3 and BFM1−2 is described in Schemes 1 and 2. This approach allowed the generation of TFMs and BFMs with uniform composition and high purity (>95% purity; the fully described synthesis, aqueous solubility, and HPLC purity analysis of TTR ligands, TFMs, and BFMs can be found in the Supporting Information).

In Silico Modeling Studies. The geometry optimization of the ligand **2**, **3**, **4**, and TFM3 was carried out at the hybrid density functional B3LYP level[11] with 6-31G(d)[12,13] basis set using Gaussian 09[14] program package. To confirm the optimized geometry is at minimum, frequency calculations were carried out on the optimized geometries. The docking experiments were carried out using Dock6.[15] The crystal structure of TTR (pdb id: 4HIQ)[10] and the PSMA (pdb id: 2XEF)[16] were obtained from RCSB.org. UCSF Chimer program[17] was used to analyze and visualize the proteins and docking complex structures. Because of the large size of TFM3, smaller versions of the ligands were prepared for the docking. After docking PSMA and TTR with TFM3, the best protein−ligand docking complex was identified for each protein and they were superimposed onto the full TFM3 anchoring both ligand **2** and **22** conjugated to vcMMAE.

Evaluation of Binding Affinity of Ligands to TTR in Buffer. The affinity of **2**, **3**, **4** and TFM1−3 to TTR was determined by their ability to displace FP probe from TTR using previously reported fluorescence polarization (FP) assay.[18] Serial dilutions of **2**, **3**, **4**, and TFM1−3 (0.010 μM to 20 μM) were added to a solution of FP-probe (50 nM) and TTR (300 nM) in assay buffer (PBS pH 7.4, 0.01% Triton-X100, 1% DMSO in 25 μL final volumes) in 384-well plate. The samples were allowed to equilibrate by agitation on a plate shaker for 20 min at room temperature. Fluorescence

DOI: 10.1021/acs.molpharmaceut.9b00432
Mol. Pharmaceutics 2019, 16, 3237−3252

Scheme 2. Synthesis of BFM2, TFM2, and TFM3: TTR Ligand 2 (Blue), PSMA Ligand (Black), Payload (MMAE in Red), and Linker System (Magenta)

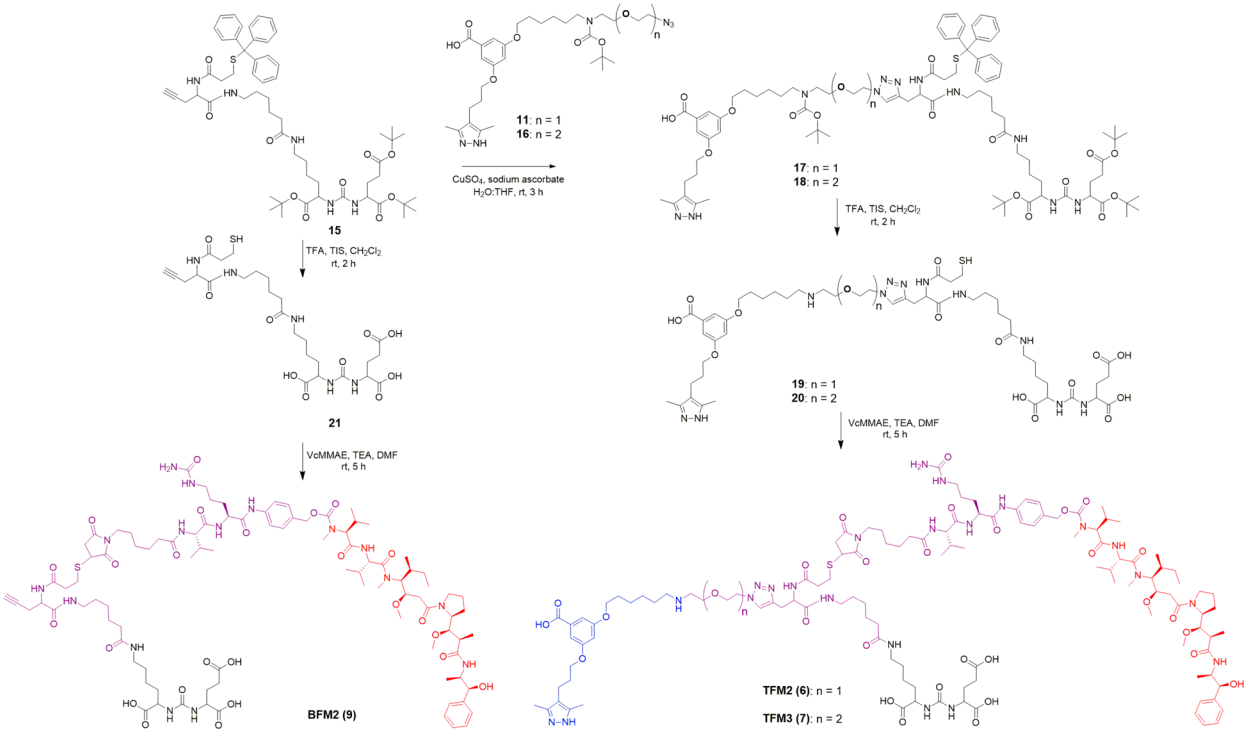

polarization (excitation λ 485 nm, emission λ 525 nm, Cutoff λ 515 nm) measurements were taken using a SpectraMax M5Microplate Reader (Molecular Devices). The IC_{50} values were obtained by fitting the data to the following equation [$y = (A - D)/(1 + (x/C)^B) + D$], where A = maximum FP signal, B = slope, C = apparent binding constant (K_{app}), and D = minimum FP signal. The binding constant (K_d) values were calculated using the Cheng–Prusoff equation from the IC_{50} values. All reported data represent the mean ± s.d. (n = 3).

Evaluation of Binding Affinity and Selectivity of Ligands to TTR in Human Serum. The binding affinity and selectivity of ligands **2**, **3**, **4**, and TFM1–3 to TTR were determined by their ability to compete with the binding of a fluorescent probe exclusion (FPE probe) binding to TTR in human serum as previously reported.[19,20] AG10 and Tafamidis were used as controls. An aliquot (98 μL) of human serum was mixed with 1 μL of test compounds (1.0 mM stock solution in DMSO; 10 μM final concentration in serum) and 1 μL of FPE probe (0.36 mM stock solution in DMSO; 3.6 μM final concentration in serum). The fluorescence changes (λ_{ex} = 328 nm and λ_{em} = 384 nm) were monitored every 15 min using a SpectraMax M5 microplate reader for 6 h at 25 °C.

PSMA Enzyme Inhibition Assay for Evaluating the Preferential Binding of TFM1–3 for PSMA over TTR. Test compounds (TFM1–3 and BFM1–2) were assayed for their ability to inhibit PSMA-catalyzed hydrolysis of N-acetylaspartylglutamate (NAAG) to glutamate and N-acetylaspartate (NAA) in the PSMA enzyme inhibition assay using the Amplex Red Glutamic Acid/Glutamate Oxidase Assay Kit. PMPA and ligand **22** were used as positive controls. A 10 mM solution of N-acetylaspartylglutamate (NAAG; MP Biomedicals, ICN15303625) in 40 mM NaOH was diluted to 40 μM in reaction buffer (0.1 M Tris·HCl, pH 7.5), and the solution was added to a 384-well plate (10 μL per well). To measure PSMA/NAAG K_m, the NAAG solution was serially diluted (2×) to obtain final NAAG concentrations ranging from 390 nM to 100 μM (prepared from the 10 mM stock). For IC_{50} measurements, the inhibitors in reaction buffer containing 40 μM NAAG solution were serially diluted (4× with buffer containing 40 μM NAAG) to obtain final inhibitor concentrations ranging from 1.5 nM to 100 μM. To evaluate the ligands ability to inhibit PSMA in the presence of transthyretin, TTR was also added (at 1 μM final concentration) to the test compounds. To initiate reactions, *rh*PSMA (20 μM in reaction buffer), was added to each well to a final concentration of 60 ng/mL. The plate was incubated at 37 °C for 30 min and then was heated to 90 °C for 1 min. After cooling, Amplex reaction mixture was added at a 1:1 volumetric ratio and incubated at 37 °C for 1 h. Fluorescence intensities were measured using a SpectraMax M5 microplate reader with excitation and emission filters of 545 and 590 nm, respectively. K_i values were calculated using the Cheng–Prusoff equation from IC_{50} and K_m values (calculated using GraphPad Prism 8 software). All reported data represent the mean ± s.d. (n = 3).

In Vitro Analysis of Efficacy of MMAE Release Following Cathepsin B Cleavage. Cathepsin B, extracted from human liver, was obtained frozen at 15.5 μM in 20 mM sodium acetate and 1 mM EDTA at pH 5.0. The enzyme was incubated with 25 mM sodium acetate, 1 mM EDTA, and 9.2 mM DTT at pH 5.5 for 15 min at ambient temperature for activation. In the MMAE release assay, the activated cathepsin B at a final concentration of 100 nM was mixed with free MMAE, BFM2, TFM2, and TFM3 at a final concentration of 20 μM in the reaction buffer (25 mM sodium acetate and 1 mM EDTA at pH 5.5) at 37 °C. Sample aliquots were taken at 0, 15 min, 30 min, 1 h, and 2 h. Each aliquot of sample was immediately quenched by adding HPLC solvent (acetonitrile–

DOI: 10.1021/acs.molpharmaceut.9b00432
Mol. Pharmaceutics 2019, 16, 3237–3252

water; 95:5 v/v, 0.1% formic acid), mixed by vortexing, placed at −20 °C for 5 min, centrifuged at 15 000 rpm for 5 min, and the supernatant was analyzed by HPLC (gradient method increasing linearly from 0 to 100% solvent B in 20 min) for quantifying the release of free MMAE. HPLC detection was performed at 210 nm UV absorbance because of the low absorbance of MMAE at 254 nm. The identity of MMAE was also confirmed by LC−MS/MS.

Evaluating Effect of TTR on Cytotoxicity of TFMs Against Prostate Cancer Cells. 3-(4,5-Dimethylthiazol-2-yl)-2,5-diphenyltetrazolium bromide (MTT) assay was performed using CellTiter 96 Non-Radioactive Cell Proliferation Assay to determine cell viability. LNCaP (PSMA+), DU145 (PSMA−), and HeLa cells were cultured in RPMI-1640 medium supplemented with 10% fetal bovine serum, penicillin/streptomycin (100 unit/mL and 100 μg/mL, respectively), and 1% L-glutamine under the humidified atmosphere of 5% CO_2 and 95% air at 37 °C. The cells were grown to confluence, trypsinized, and seeded into 96-well plates at a density of ∼5000 cells/well. The cells were then treated with BFM2, TFM2, TFM3 (each at 0.001 nM to 100000 nM), or MMAE (0.001 nM to 1000 nM) as positive control in absence and presence of TTR (1 μM, 30 min preincubation with test compounds). Control cells were also treated with the appropriate concentration of vehicle (DMSO) in absence and presence of TTR (1 μM, 30 min preincubation). After 72 h incubation at 37 °C, cell viability was determined following the standard CellTiter 96 Non-Radioactive Cell Proliferation Assay protocol.

Evaluating Effect of TFM3 on Holo-RBP−TTR Interaction in Serum. A solution of thyroxine (T_4), ligand **2**, and TFM3 (1 μL of 2 mM stock solution in DMSO) or control (1 μL DMSO) was added (final compound concentrations 20 μM) to 99 μL of human serum (from human male AB plasma, Sigma; TTR concentration ∼5 μM). The treated serum was incubated at 37 °C for 2 h. After the incubation, all samples were analyzed using Western blot using a procedure reported earlier.[9] In this assay, 10 μL of the serum incubated with test compounds was added to 90 μL of buffer A (pH 7.0 PBS, 100 mM KCl, 1 mM EDTA, 1 mM DTT). For the urea sample, 10 μL of the control serum (incubated with DMSO) was added to 90 μL of urea buffer (buffer A containing 8 M urea). All serum samples were then cross-linked with glutaraldehyde (final concentration of 2.5%) for 5 min, and then quenched with 10 μL of 7% sodium borohydride solution in 0.1 M NaOH. The samples were denatured by adding 100 μL of SDS gel loading buffer and boiled for 5 min. Ten microliters of each sample was separated in 16% SDS-PAGE gels. The gel was transferred using wet transfer (Bio-Rad; buffer: 3.03 g of Tris, 14.4 g of glycine, 200 mL methanol, 800 mL water). Membrane was blocked in blocking buffer (Sea-block blocking buffer, Fisher) for 30 min at room temperature. The membrane was then incubated in anti-RBP antiserum at 1:500 dilution overnight at 4 °C. After incubation, the membrane was washed four times for 5 min each in 0.1% Tween-20 PBS at room temperature. Then the membrane was incubated in IRdye800 donkey antirabbit secondary antibody at 1:15 000 dilution in blocking buffer for 2 h at room temperature. After incubation, the membrane was washed in similar manner as above and scanned using a LI-COR Odyssey CLx Imaging System for quantification. The free RBP band (at ∼21 kDa) was quantified easily since it was well separated from the RBP−TTR complex (at ∼77 kDa), which is also detected by the anti-RBP antiserum.

Experimental Animals. All rats and mice animal studies and euthanasia were conducted in accordance with National Institutes of Health guidelines for the care and use of live animals and were approved by the Institutional Animal Care and Use Committee at University of the Pacific.

Evaluation of Pharmacokinetic Profile of BFM1, TFM1, BFM2, and TFM3 in Rats. Jugular vein cannulated male Wistar rats (200−220 g; 6−7 weeks old) were used for this study. Animals were randomized in four treatment groups (n = 3 animals per group for BFM1 and TFM1; n = 4 animals per group for BFM2 and TFM3). Each animal received one intravenous dose of either BFM1 (0.1 μmol/kg), TFM1 (0.1 μmol/kg), BFM2 (0.32 μmol/kg), or TFM3 (0.16 μmol/kg) in 200 μL saline through the jugular vein cannula. Blood samples were collected from each rat, via jugular vein cannula, in heparinized tubes at predetermined time points (0.083, 0.25, 0.5, 1, 2, 4, 6, 8, 12, and 24 h postdosing), and the volume was replaced with sterile normal saline. The plasma samples were prepared by centrifugation at 7500 rpm for 15 min at 4 °C and stored at −80 °C until further analysis. For BFM1 and TFM1, the plasma samples were diluted with PBS in a black 96-well microplate with a clear bottom. LI-COR Odyssey CLx Imaging System was used to quantitate the concentration of BFM1, and TFM1 in rat plasma. The fluorescence intensity of each compound was determined in the 800 nm channel. The integrated intensity automatically quantified by LI-COR Odyssey CLx Imaging System, for each sampling time point, was converted to nM concentration by the calibration curves produced from the calibration samples of each compound (Figure S4). For BFM2 and TFM3, to each of the plasma samples of the standard curve, 2× volume of 100% acetonitrile was added to precipitate the proteins in the rat plasma. The samples were vortexed for 30 s then placed on a mechanical shaker for 10 min at medium speed. The samples were then centrifuged at 15 000 rpm for 10 min; the supernatant was collected and centrifuged again at 15 000 rpm for another 10 min. Subsequently, the supernatant was analyzed using validated LC−MS/MS method (using Triple Quadrupole mass spectrometer; AB SCIEX API-3000) to quantitate the concentration of BFM2 and TFM3 in plasma samples. Fragmentation pattern and peak areas were used to identify and quantitate the test compounds, respectively. On the basis of a calibration curve for these compounds in rat plasma and the internal standard generated by the LC−MS/MS analyst, the concentrations in the plasma samples were then plotted as their natural logarithms against time (Figure S11). A two compartment model (using WinNonlin) was used to obtain all the pharmacokinetic parameters. Mean (±s.d.) concentrations of BFM1, TFM1, BFM2, and TFM3 in the plasma samples were plotted as their natural logarithms against time (h). A two-compartment model (using Phoenix WinNonlin) was used to obtain all the pharmacokinetic parameters for test compounds from their plasma concentration−time data.

In Vivo Toxicity Study in Mice. Five-week-old CD-1 male mice (Charles River) were randomized into groups (n = 4) with similar mean body weight. The mice received either vehicle (5% Ethanol, 10% PEG 400 and 85% sterile water), TFM3 (300 nmol/kg and 600 nmol/kg), BFM2 (300 nmol/kg and 600 nmol/kg), or MMAE (300 nmol/kg) via intraperitoneal injection (i.p.), every 3 days, total four doses. Body weight and food and water intake were recorded every 3 days

DOI: 10.1021/acs.molpharmaceut.9b00432
Mol. Pharmaceutics 2019, 16, 3237−3252

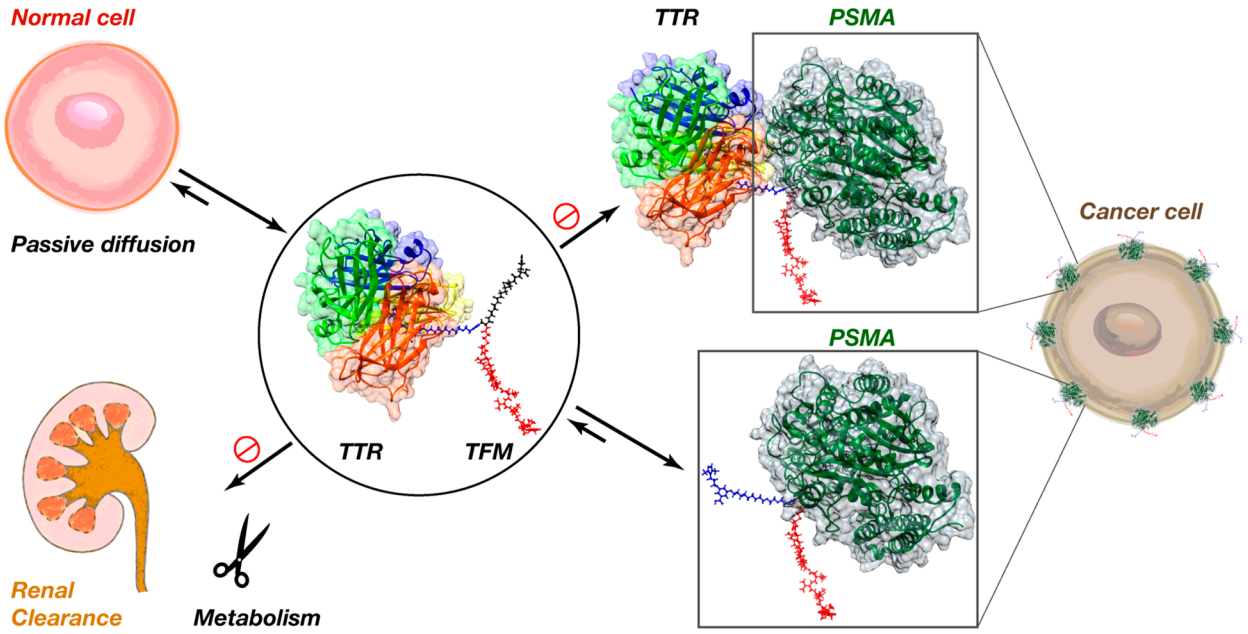

Figure 2. Schematic illustration of the concept for the TTR-based targeted drug delivery approach. TFMs comprise TTR binding ligand (blue), PSMA ligand (black), and Payload (Cy7 or MMAE in red). The hydrophilic TTR ligand allow TFMs to bind reversibly to circulating TTR, thereby reducing its renal clearance and enhancing its in vivo $t_{1/2}$. The overall hydrophilic nature of TFMs, in addition to binding to TTR, would also reduce the nonselective tissue distribution of TFMs to normal cells. The PSMA targeting module allows the TFMs to selectively deliver the therapeutic payload of these TFMs to its intracellular targets in PSMA+ prostate cancer (PCa) cells. The binding affinity of TFMs to PSMA is higher than its binding to TTR, which allows the TFMs to preferably interact with PSMA over TTR. The linker system we used is too short to bring the two proteins in close proximity to each other, which prevents the formation of the ternary complex.

for 12 days. Body weight changes from the beginning of treatment for the animals were calculated as mean (±s.d.) % change from day 0 for each group.

Xenograft Tumor Model Generation. LNCaP (PSMA+) and DU145 (PSMA−) cells (PCa cells) were cultured in RPMI-1640 medium supplemented with 10% fetal bovine serum, penicillin/streptomycin (100 unit/mL and 100 μg/mL, respectively) and 1% L-glutamine under the humidified atmosphere of 5% CO_2 and 95% air at 37 °C. The cells were grown to confluence, trypsinized, and washed twice with cold HBSS (4 °C) and collected by centrifuging at approximately 125 × g for 10 min at 4 °C. The % viable cells were then counted using a hemocytometer and trypan blue (final concentration 0.32%). Male athymic nude mice (nu/nu, 5-week-old, Charles River) were subcutaneously injected with 5 × 10^6 LNCaP (PSMA+) cells or 1 × 10^6 DU145 (PSMA−) cells, suspended in 100 μL of 1:1 (v/v) HBSS/Matrigel (Becton Dickinson) mixture, on both flanks. Tumor volumes were measured with digital caliper every 3 days and calculated as V = (L × W^2)/2 assuming ellipsoid tumor shape. When the tumor volume reached 100−150 mm^3 (10−14 days), the mice were randomized into groups with similar mean tumor volume for in vivo imaging and efficacy studies.

In Vivo Imaging and Biodistribution Study in Mouse Xenograft Model. Mice (n = 3) bearing LNCaP (PSMA+) and DU145 (PSMA−) tumors received either vehicle (1% DMSO, 99% sterile saline), TFM1 (17 nmol/kg), or BFM1 (17 nmol/kg) in vehicle via tail vein injection. In vivo fluorescence imaging was performed on one animal from each group together for both tumor models at 1, 4, 24, 48, and 72 h postinjection on LI-COR Odyssey CLx Imaging System at excitation and emission wavelength 685 and 800 nm, respectively. After 72 h, animals were sacrificed and tumors, liver, kidney, heart, and blood were collected, rinsed with PBS buffer, and weighed. Ex vivo fluorescence imaging and quantitative analysis were performed on the collected organs for biodistribution study using LI-COR Odyssey CLx Imaging System and Image Ready software supplied with the instrument. Mean (±s.d.) AFU/mg values were calculated for all collected organs and blood.

In Vivo Efficacy in Mouse Xenograft Model. Mice (n = 6) bearing LNCaP (PSMA+) and DU145 (PSMA−) tumors received either vehicle (5% ethanol, 10% PEG 400, and 85% sterile water) or test compounds (either TFM3, BFM2, or MMAE, at a dose of 300 nmol/kg) in vehicle via intraperitoneal injection, every 3 days, total four doses. Body weight, tumor volumes, and food and water intake were recorded every 3 days for 14 days. After 14 days, animals were sacrificed, and all tumors were excised and weighed.

Statistical Analysis. All results are expressed as mean ± s.d. Statistical analysis was performed with GraphPad PRISM 8 software. The significance of the differences were measured by one-way ANOVA followed by Tukey's multiple comparison test (ns, not significant; $*p \leq 0.05$; $**p \leq 0.01$; $***p \leq 0.001$; $****p \leq 0.0001$).

RESULTS AND DISCUSSION

General Concept of TTR-Based Targeted Drug Delivery System. LTDs are typically bifunctional molecules (BFMs) that include a targeting ligand chemically linked to a therapeutic cytotoxic payload or imaging agent through a linker. To overcome the poor pharmacokinetics of BFMs, while maintaining their hydrophilicity and small size, we outfitted these BFMs with an additional arm containing the hydrophilic TTR binding ligand (i.e., forming trifunctional

DOI: 10.1021/acs.molpharmaceut.9b00432
Mol. Pharmaceutics 2019, 16, 3237−3252

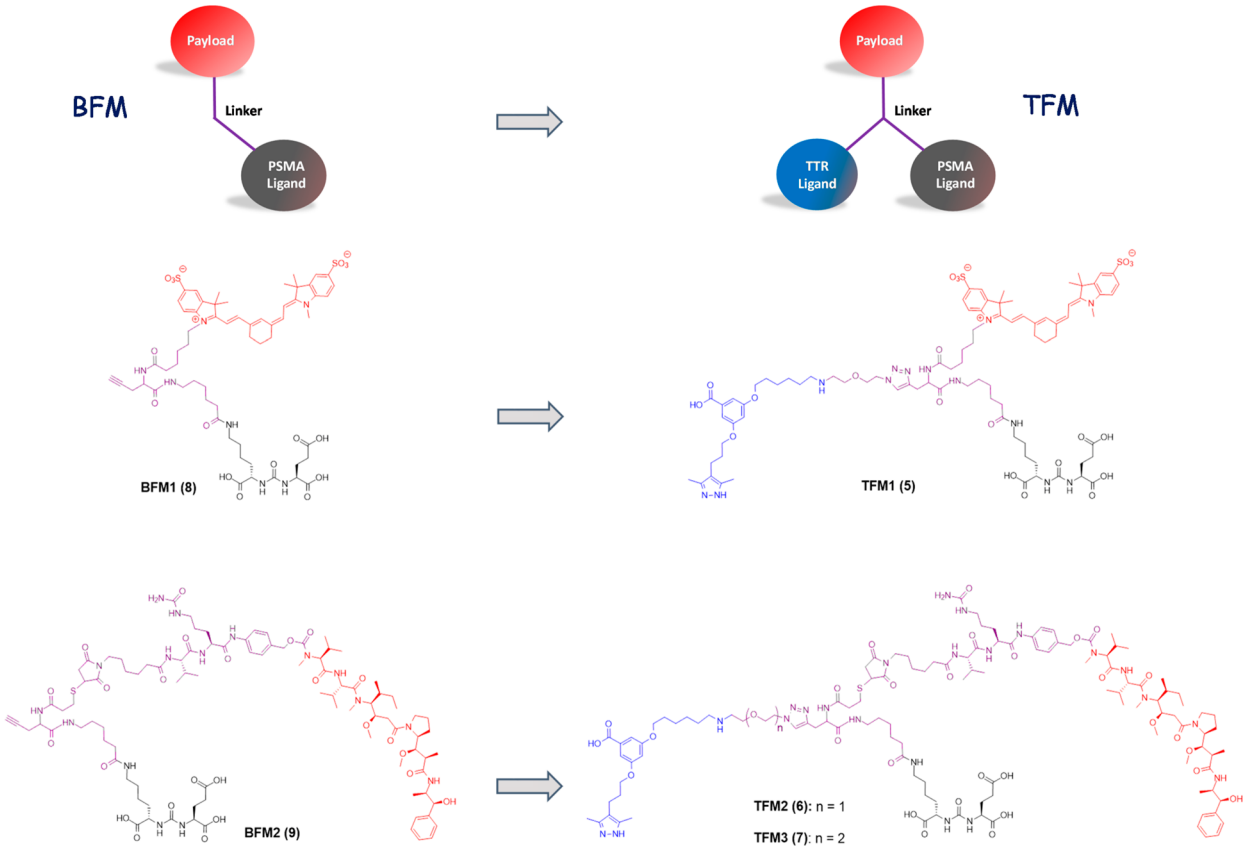

Figure 3. Chemical structures of TFMs and BFMs. TFMs are composed of four modules; TTR ligand **2** (blue), PSMA ligand (black), Payload (Cy7 or MMAE in red), and linker system (magenta). BFM1 and TFM1 incorporate the imaging dye Cy7 attached through a noncleavable linker. MMAE was incorporated in BFM2, TFM2, and TFM3 via a valine−citrulline dipeptide cleavable linker. TFM3 has a slightly longer PEG spacer that increases its hydrophilicity compared to TFM2.

molecules, TFMs). To establish the proof of concept, we designed these TFMs to deliver a hydrophilic small molecule imaging agent, Sulfo-Cyanine7 (Cy7; a water-soluble indocyanine 7 dye for near-infrared (NIR) in vivo imaging) or a lipophilic cytotoxic agent (monomethyl auristatin E, MMAE) to PCa cells overexpressing the prostate-specific membrane antigen (PSMA) (Figure 2). PSMA is a transmembrane protein that is largely absent from healthy tissues but highly expressed on the surface of PCa cells and on new blood vessels that supply nutrients to many other types of cancers.[21,22] PSMA is also highly overexpressed in metastatic castration-resistant prostate cancer (mCRPC), and therefore, targeting PSMA is considered a promising target both for imaging and chemotherapeutic agents.[23−25]

Development of Second-Generation Hydrophilic TTR Ligands. We hypothesized that incorporating hydrophilic spacers in the TTR ligands will maintain the overall hydrophilicity of TFMs, limiting their passive diffusion into PSMA-negative cells. To assess the positions on linker system of the TTR ligands that could be amenable for modification, we performed in silico modeling studies that were focused on identifying possible interactions that could be formed between our new hydrophilic linkers and T_4 pocket of TTR. Our modeling studies suggested that by incorporating an amine group in linker we would accomplish two goals: (1) the amine group could potentially form an ionic interactions (salt bridges) with the two glutamic acid residues (Glu54/Glu54′) close to the surface of TTR; (2) the amine group will be highly protonated under physiological pH, which would increase the hydrophilicity of the new TTR ligands. This modification would not only increase the affinity of the new ligands to TTR but would also increase the selectivity for TTR in serum by decreasing nonspecific interactions with other serum proteins such as albumin. Modeling studies suggest that a linker length of ∼8 Å will be needed to project the amine group close to Glu54/Glu54′. The study showed that the putative salt bridges between the amine group and Glu54/Glu54′ do not interfere with the major interactions (salt bridges between the carboxylate of ligand **2** and the ε-amino groups of Lys15 and Lys15′ and hydrogen bonds between the pyrazole nitrogens of **2** and Ser117 and Ser117′ of TTR) between the AG10 portion of the TTR ligand and inner TTR pocket (Figure 1b). Therefore, we attached the amine group through a six carbon linker to the meta-position of AG10 to give TTR ligand **2** (Figure 1b). To investigate the hypothesized salt bridges with Glu54/Glu54′, we also tested the t-Boc-protected version of **2** that cannot form salt bridges with Glu54/Glu54′ (compound **3**, Figure 1c). The binding affinity of ligand **3** to TTR was significantly lower than the binding affinity of ligand **2** (discussed further). To investigate the effect of the steric bulk of the t-Boc group on the lower affinity, we also synthesized ligand **4** (containing a secondary amine group; Figure 1d) where short ethylene glycol spacer was added to **2**. Ligand **4** maintained very good binding affinity and selectivity to TTR in buffer and serum, supporting the formation of the hypothesized salt bridges. Therefore, we decided to use the hydrophilic ligand **2** as the main TTR binder in the synthesis of our TFMs.

DOI: 10.1021/acs.molpharmaceut.9b00432
Mol. Pharmaceutics 2019, 16, 3237−3252

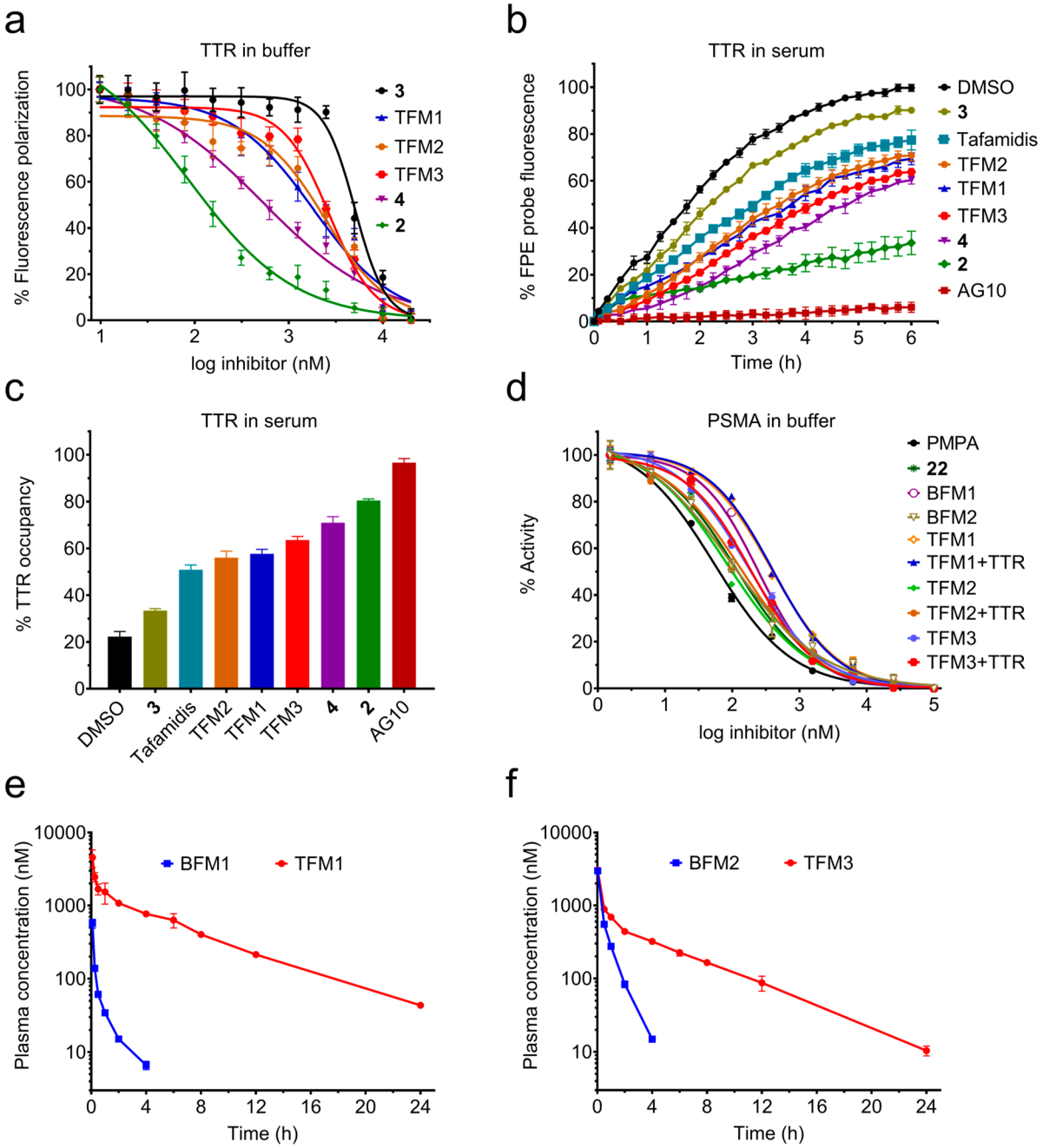

Figure 4. Binding affinity of TFMs to TTR and PSMA in buffer and human serum and effect of TTR on extending the $t_{1/2}$ of TFM1 and TFM3 in rats. (a) Evaluation of the binding affinity of test compounds (0.01 μM to 20 μM) to TTR in buffer using fluorescence polarization assay. The binding constant (K_d) values were calculated using the Cheng–Prusoff equation from IC_{50} values. Data represent the mean ± s.d. (n = 3). (b) Fluorescence change caused by modification of TTR in human serum (TTR concentration, ~5 μM) by covalent FPE probe monitored for 6 h in the presence of FPE probe alone (black circles) or probe and TTR ligands (colors; 10 μM). The lower the binding and fluorescence of FPE probe, the higher is the binding selectivity of ligand to TTR. (c) Bar graph representation of percent occupancy of TTR in human serum by TFMs in the presence of FPE probe measured after 3 h of incubation relative to probe alone. Error bars indicate mean ± s.d. (n = 4). (d) Evaluation of the inhibitory activity of test compounds (1.5 nM to 100 μM) on PSMA-catalyzed cleavage of N-acetylaspartylglutamate (NAAG). K_i values were calculated using the Cheng–Prusoff equation from IC_{50} and K_m values. Data represent the mean ± s.d. (n = 3). (e, f) Pharmacokinetic properties of test compounds were evaluated in male Wistar rats. (e) Single intravenous bolus dose of TFM1 or BFM1 (0.1 μmol/kg) was administered to two groups of male rats (n = 3 for each group). The concentration of test compounds in plasma was determined at different time points. Concentrations are expressed as means ± s.d. of three biological replicates. (f) BFM2 (0.32 μmol/kg) and TFM3 (0.16 μmol/kg) were evaluated following a single intravenous bolus dose to two groups of male rats (n = 4 for each group). The concentration of test compounds in plasma was determined at different time points. Concentrations are expressed as means ± s.d. of four biological replicates.

Design and Synthesis of TFMs and BFMs. The basic structure of the TFMs was intended to bring together four modules in a single construct: (i) TTR Ligand **2**; (ii) PSMA targeting ligand; (iii) therapeutic/diagnostic payload; (iv) linker system. We have designed and synthesized three TFMs (TFM1–3; Figure 3). TFM1 (**5**) has the imaging dye Cy7

DOI: 10.1021/acs.molpharmaceut.9b00432
Mol. Pharmaceutics 2019, 16, 3237–3252

attached through a noncleavable linker for diagnostic purpose. TFM2 (**6**) and TFM3 (**7**) have MMAE, which is a highly potent hydrophobic antimitotic agent that inhibits cell division by blocking tubulin polymerization, with TFM3 having a slightly longer and more hydrophilic spacer than TFM2. Because of dose-limiting toxicities, MMAE is too toxic to be administered in its untargeted forms. However, MMAE is an established targeted drug for a number of clinically used ADCs such as Adcetris.[26] MMAE was incorporated in TFM2 and TFM3 via a valine-citrulline dipeptide cleavable linker, a standard linker widely used in many successful ADCs including Adcetris.[27] The linker is designed to be stable in the bloodstream and then release the active MMAE only when the TFMs are internalized into the targeted cancer cell's endosome. In all TFMs, we incorporated a known glutamate-urea-lysine ligand for targeting PSMA. Glutamate-ureas are low-molecular weight and high affinity PSMA ligands, which selectively bind and then enter PSMA-expressing cells by PSMA endocytosis.[28,29] These ligands have been widely used for targeting both diagnostic and therapeutic agents to PSMA expressing PCa cells. The total length of the spacer and linker system required for TFMs was determined from the distance between the proximal end of the bound Glutamate-ureas and TTR ligand to the unobstructed protein surface of PSMA and TTR, respectively (discussed below). As controls for typical LTDs, we also synthesized two control BFMs: (i) BFM1 (**8**): a conjugate of the dye, Cy7, and the PSMA ligand connected through a noncleavable linker; and (ii) BFM2 (**9**): a conjugate of MMAE and the PSMA ligand connected through a valine-citrulline cleavable linker (Figure 3). Since BFM1 and BFM2 lack the TTR ligand **2**, they would allow us to evaluate the effect of TTR recruitment on the performance of our TFMs.

We have developed an efficient modular approach for the synthesis of TFM1−3 and BFM1−2 (Schemes 1 and 2). Short ethylene glycol spacers were initially attached to ligand **2**, which was required to clear the thyroxine (T_4) binding site of TTR. In addition, ethylene glycol spacers would further enhance the hydrophilicity of ligand **2**. The terminal end of the spacers was equipped with an azide group, which was used to construct the TFMs by click coupling with an alkyne group that was introduced on the PSMA ligand. This approach allowed the generation of TFMs with uniform composition and high purity (>95% purity; the fully described synthesis and HPLC purity analysis of TTR ligands, TFMs, and BFMs can be found in the Supporting Information).

Evaluation of Binding Affinity and Selectivity of Ligand 2 and TFM1−3 to TTR in Buffer and Serum. The binding affinity (K_d) of ligand **2** and TFM1−3 to human TTR was evaluated using fluorescence polarization (FP) binding assay.[18] Ligand **2** binds TTR with high affinity (K_d = 48.9 nM; Figure 4a), which could be due to the ability of **2** to form salt bridges with Glu54 (Figure 1b). The putative salt bridges between the amine of **2** and Glu54 were also supported by the significant difference between the binding affinity of ligands **3** and **4**. While there was a 20-fold decrease in binding of **3** (where the amine group is masked by a t-Boc group) to TTR (K_d = 1040 nM), ligand **4** maintained very good binding affinity (K_d = 107.5 nM). The binding affinity of TFM2 to TTR (K_d = 497.7 nM) was similar to that of TFM3 (K_d = 553.4 nM), while the binding affinity of TFM1 was slightly higher (K_d = 374.1 nM) (Figure 4a). It is clear that attaching the MMAE or Cy7 to **2** resulted in lower binding affinity to TTR. However, this decrease in TTR binding affinity might be useful for allowing the molecules to preferably interact with PSMA.

For our approach to work in vivo, TFMs must be able to selectively bind to TTR in the presence of >4000 other human serum proteins. We evaluated the selectivity of ligand **2** and TFM1−3 binding to TTR in human serum using a well-established TTR serum fluorescent probe exclusion (FPE) selectivity assay.[19,20] The FPE assay is based on employing a fluorescent conjugate competition assay using a probe (covalent-probe) that binds selectively to TTR in serum and then covalently modifies the Lys15 amino acid at the periphery of the T_4 pocket, creating a fluorescent conjugate. Ligands that bind selectively to TTR in serum decrease the binding of covalent-probe to TTR, thus lowering the fluorescence. Our data showed that ligands **2** and **4** had a much higher TTR occupancy (80.4 ± 0.7% and 71 ± 2.6%, respectively) compared to compound **3** (33.4 ± 0.8%) (Figure 4b,c). TFM1, TFM2, and TFM3 maintained very good binding selectivity to TTR in serum (57.6 ± 1.9%, 56.1 ± 2.8%, and 63.6 ± 1.6% TTR occupancy, respectively). The lower performance of TFMs in the FPE assay, compared to that of ligands **2** and **4**, is more likely due to the lower binding affinity of TFMs to TTR and possibly some binding to other serum proteins. Importantly, the performance of all TFMs was similar or better than that of TTR stabilizer, tafamidis[30] (an approved drug for TTR amyloidosis; 50.8 ± 2.0% TTR occupancy) (Figure 4b,c).

Evaluation of Binding Affinity of TFM1−3 to PSMA and Ability of TFM1−3 To Preferentially Interact with PSMA in the Presence of TTR. TFMs must first bind to TTR in serum but should also be able to leave TTR and bind to PSMA on the surface of PCa cells. This could be a mutually exclusive binding which is governed by the equilibrium constants of TFMs to TTR and PSMA (the desired outcome, assuming TFMs binding affinity is higher for PSMA than for TTR) or TFMs could bind both TTR and PSMA at the same time resulting in a drop in binding potency (the undesired outcome that is analogous to the PEGylation approach). Therefore, we tested the ability of TFM1−3 to preferentially bind to PSMA over TTR.

We used a standard PSMA enzymatic inhibition assay to test the activity of TFM1−3 (Figure 4d). This assay measures the ability of test molecules to bind and inhibit (K_i) PSMA-catalyzed cleavage of the peptide substrate N-acetylaspartyl-glutamate (NAAG). The activity of the spacer-modified glutamate-urea-lysine ligand **22** (Figure S1) on PSMA (K_i of 9.5 nM) was close to that of the potent and selective PSMA competitive inhibitor, PMPA (K_i = 4.5 nM). The bifunctional molecules, BFM1 and BFM2, also bind to PSMA with high affinity (BFM1 K_i = 20.7 nM and BFM2 K_i = 7 nM). There was a decrease in the binding affinity of TFM1 (with Cy7) to PSMA (K_i = 32.8 nM). The binding affinity of TFM1 to PSMA did not change when excess TTR (1 μM TTR compared to 1 nM PSMA) was present in the assay (K_i = 33.8 nM). A very similar pattern was observed for the MMAE conjugates, TFM2 (K_i = 7.2 nM and 11.3 nM in the absence and presence of TTR, respectively) and TFM3 (K_i = 14.7 nM and 16.4 nM in the absence and presence of TTR, respectively). Importantly, the binding affinity of TFM1−3 to PSMA (K_d ~7 to 33 nM) is higher than their binding to TTR (K_d for TTR ~350 to 500 nM, determined by FP above), which should enable the TFMs to leave TTR in serum and bind to PSMA on the surface of PCa cells.

DOI: 10.1021/acs.molpharmaceut.9b00432
Mol. Pharmaceutics 2019, 16, 3237−3252

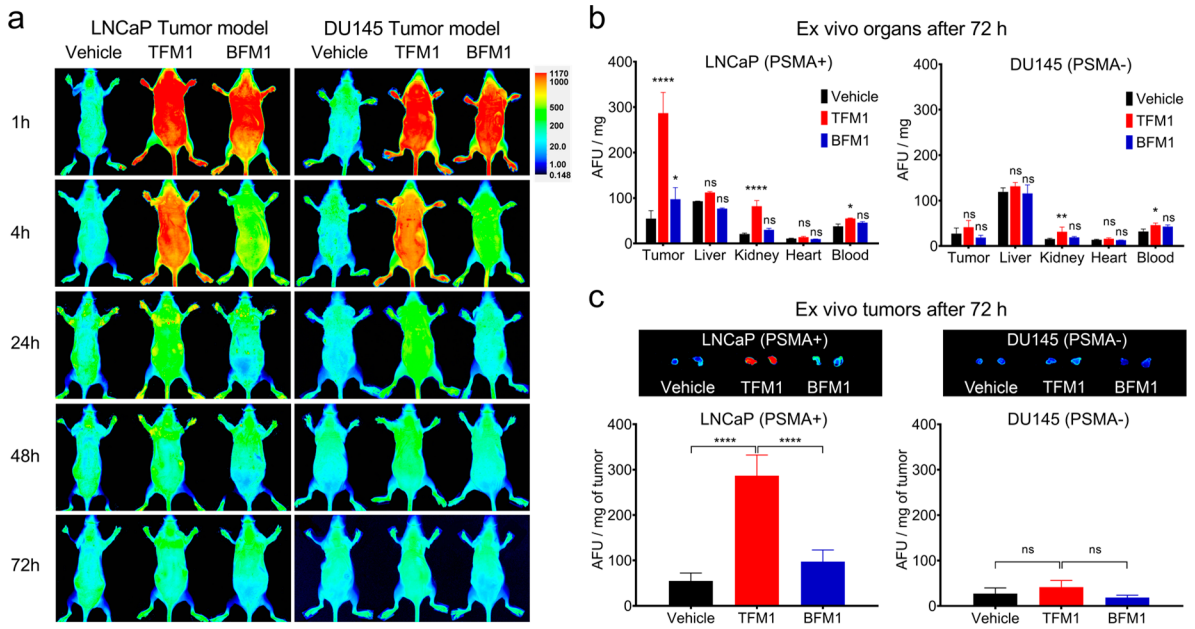

Figure 5. In vivo fluorescence imaging and ex vivo biodistribution and tumor targeting analysis of TFM1 in a xenograft mouse models of human metastatic prostate cancer. (a) Representative in vivo images of male athymic nu/nu mice (n = 3) bearing LNCaP (PSMA+) or DU145 (PSMA−) tumors, injected with vehicle, TFM1, or BFM1 at a dose of 17 nmol/kg via tail vein injection and scanned at 1, 4, 24, 48, and 72 h using LI-COR Odyssey CLx Imaging System at excitation and emission wavelength 685 and 800 nm, respectively. (b) 72 h postinjection, mice were sacrificed, and ex vivo tissue biodistribution analysis was performed by imaging of the excised tumors, liver, kidneys, heart, and blood samples. AFU/mg of excised organs and blood after 72 h. Bar graph showing the respective mean (±s.d.) (n = 6 for tumors or n = 3 for other organs). (c) Representative ex vivo images of excised LNCaP and DU145 tumors after 72 h and bar graph showing the respective mean (±s.d.) AFU/mg of excised tumors (n = 6). The significance of differences was measured by one-way ANOVA followed by Tukey's multiple comparison test (ns, not significant; $*p \leq 0.05$; $**p \leq 0.01$; $***p \leq 0.001$; $****p \leq 0.0001$).

We do not anticipate that a major fraction of TFMs could bind to PSMA and TTR simultaneously. The formation of such ternary complex would have resulted in a large decrease in the binding affinity of TFMs to PSMA when the bulky TTR (56 kDa) is present. In addition, modeling studies of TFM3 with both TTR and PSMA suggested that the linker we used (~16 Å) is too short to bring the two proteins in close proximity to each other (a linker of at least 21 Å is required to form the ternary complex between TTR, PSMA, and TFM3, Figure S2 and S3).

TTR Extended Circulation $t_{1/2}$ of TFM1 in Rats. Rat and mouse TTR (conc. in both ~ 5 μM)[31,32] have ~80% sequence homology with human TTR at the protein levels.[33,34] Most of the sequence differences occur in peripheral loop regions, while all the amino acids in the T_4 binding sites, where TFMs bind, are conserved between rat, mouse, and human. Therefore, we do not expect appreciable differences in the binding of TFMs between human and rat or mouse TTR. In addition to increasing the metabolic stability of TFMs in blood, we hypothesize that binding to TTR will also reduce glomerular filtration of TFMs due to the large size of TTR:TFM complex (~58 kDa).

We have evaluated the pharmacokinetic properties of TFM1 and BFM1 (both containing the Cy7 dye with noncleavable linker) in rats. TFM1 and BFM1 (typical bifunctional ligand-targeted molecule; i.e., TFM1 without ligand **2**) were administered as single IV doses (0.1 μmol/kg) to two groups of jugular vein cannulated male rats (Figure 4e). Blood samples were withdrawn from the jugular vein cannula at predetermined time points (ranging from 5 min to 24 h) and concentrations of test compounds were quantitated in plasma (Figure S4). Consistent with our hypothesis, the pharmacokinetic profile of TFM1 was markedly different than BFM1. The concentrations of TFM1 were significantly higher than BFM1 concentrations at any given time. While there was no measurable amount of BFM1 after 4 h, TFM1 was still present even after 24 h (Figure 4e). There was ~6.6-fold increase in the $t_{1/2}$ of TFM1 compared to BFM1 ($t_{1/2}$ = 5.03 ± 0.18 h vs 0.76 ± 0.04 h, respectively). The mean residence time (MRT) was also ~16-fold higher for TFM1 compared to BFM1 (5.27 ± 0.35 h and 0.32 ± 0.02 h, respectively). These data strongly support and validate our approach that TTR recruitment can indeed enhance the $t_{1/2}$ and pharmacokinetic profile of TFMs in vivo.

TTR Enhanced Targeting of TFM1 to PSMA-Positive Cells in Xenograft Mouse Models of Metastatic Prostate Cancer. We evaluated the in vivo tumor specificity of TFM1 and BFM1 in mice bearing PCa tumor xenografts. Tumor models were generated by injecting LNCaP (PSMA+ lymph node prostate cancer; ~10^6 PSMA copies/cell)[35,36] and DU145 (PSMA−)[35] PCa cells subcutaneously into the flanks (left and right) of male athymic *nu/nu* mice. Once the tumor volume was 100−150 mm^3, mice were randomized in groups (with similar mean tumor volume) and injected with TFM1, BFM1 (17 nmol/kg) or vehicle (sterile saline) via tail vein injection. Whole body imaging of mice was conducted at the designated time points after injection (1, 4, 24, 48, and 72 h) using LI-COR Odyssey CLx Imaging System (Figure 5a). The in vivo imaging showed that the fluorescence signal for BFM1 in both models was significantly reduced at 4 h postinjection and reduced to the background level at 24 h. In contrast, TFM1 maintained a very high fluorescence signal at 4 h and the signal was maintained for up to 48 h postinjection. These

DOI: 10.1021/acs.molpharmaceut.9b00432
Mol. Pharmaceutics 2019, 16, 3237−3252

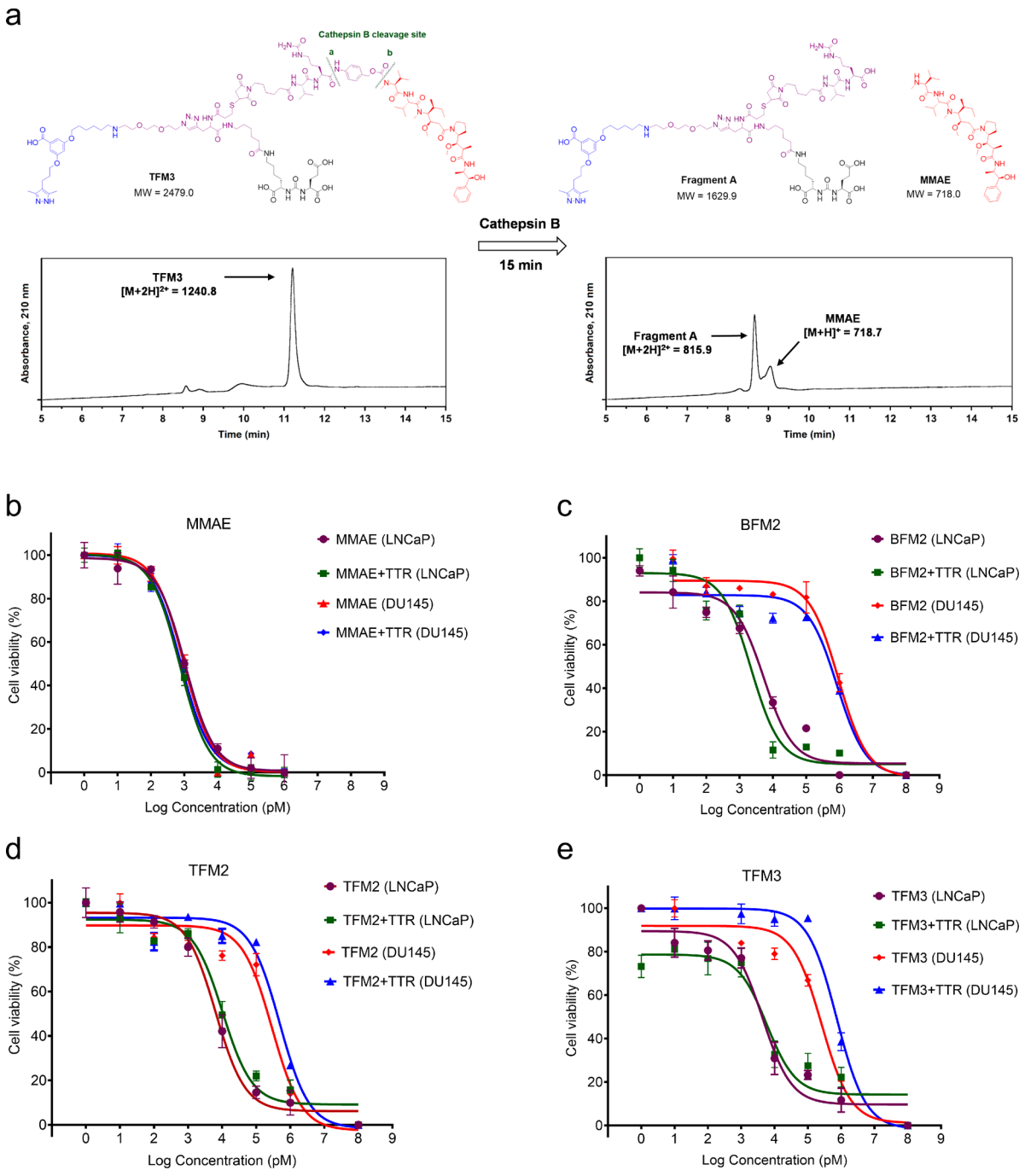

Figure 6. TFMs efficiently release MMAE after cathepsin B cleavage and have selective cytotoxicity on LNCaP (PSMA+) versus DU145 (PSMA−) cells. (a) Valine−citrulline dipeptide cleavable linker TFM3 is efficiently cleaved (within 15 min in buffer) by cathepsin B hydrolysis (step a) and spontaneous fragmentation (step b) of the para-aminobenzylcarbamate intermediate. The formation of free MMAE and Fragment A after cleavage of TFM3 was confirmed by HPLC and LC−MS/MS analysis. Similar results were obtained for cathepsin B hydrolysis of TFM2 and BFM2 as shown in Figure S5. The HPLC spectrum is a representative of triplicate experiments (n = 3). (b−e) Selective uptake of BFM2, TFM2, and TFM3 by PSMA receptors and the effect of TTR on lowering the cytotoxicity of TFM2 and TFM3 on PSMA− cells. MTT cell proliferation assay was used to determine the cytotoxicity of MMAE, BFM2, TFM2, and TFM3 against LNCaP (PSMA+) and DU145 (PSMA−) cell lines in the absence and presence of TTR. (b) MMAE shows similar cytotoxicity against LNCaP and DU145 cell lines regardless of the absence and presence of TTR. (c) Selective cytotoxicity of BFM2 against LNCaP (PSMA+) compared to DU145 (PSMA−) cell lines. The activity of BFM2 on these cell lines was similar in the absence and presence of TTR. Selective cytotoxicity of (d) TFM2 and (e) TFM3 against LNCaP (PSMA+) compared to DU145 (PSMA−) cell lines. Both TFM2 and TFM3 were less toxic against DU145 (PSMA−) cell lines in the presence of TTR. Each time point is expressed as means ± s.d. (n = 5).

data support the in vivo pharmacokinetic profile of BFM1 and TFM1 observed in rats (Figure 4e).

The mice were sacrificed 72 h postinjection, and ex vivo tissue biodistribution analysis was performed by imaging of the excised tumors, liver, kidneys, heart, and blood samples. These studies demonstrated that TFM1 and BFM1 accumulated predominantly in PSMA expressing LNCaP tumors, with no substantial fluorescence activity in other tissues except kidneys

DOI: 10.1021/acs.molpharmaceut.9b00432
Mol. Pharmaceutics 2019, 16, 3237−3252

(Figure 5b). The superior selectivity of TFM1 for PSMA+ tumors was also demonstrated by ex vivo imaging of excised tumors which showed a ∼7-fold higher fluorescent signal in LNCaP compared to DU145 tumors (Figure 5c). There was a ∼3-fold enhanced uptake of TFM1 in LNCaP compared to BFM1. This indicates that the enhanced tumor uptake of TFM1 in LNCaP (PSMA+) tumors is due to the extended circulation $t_{1/2}$ of TFM1 compared to BFM1, particularly since the binding affinity of BFM1 to PSMA in buffer was found to be higher than that of TFM1 (K_i = 20.7 nM and 33.8 nM, respectively).

TFM2 and TFM3 Efficiently Release MMAE Following Cathepsin B Cleavage in Buffer. For TFMs to efficiently deliver MMAE to the cytosol, they must be cleaved by cathepsin B inside the lysosomes of target cancer cells. An in vitro enzymatic reaction model was constructed to mimic the in vivo cathepsin B cleavage of the valine-citrulline linker connecting MMAE to TFM2 and TFM3. The efficiency of MMAE release from the intact TFMs was assessed by treating TFM2 and TFM3 with cathepsin B (isolated from human liver) in buffer (pH 5.5; optimal pH of cathepsin B, which is close to the pH in the lysosome) at 37 °C. The release of active MMAE from TFMs was analyzed by analytical HPLC as a function of time. MMAE and individual intact TFMs were injected as standards to identify the corresponding species in the reaction mixture. Incubation of BFM2, TFM2, and TFM3 (20 μM) with cathepsin B (100 nM) resulted in efficient MMAE release (98%) within 15 min (Figure 6a and Figure S5). LC−MS/MS analysis of TFM3 further confirmed the release of MMAE and a fragment that contained compound **2** and PSMA ligand.

Evaluating Effect of TTR on Cytotoxicity of TFMs against PSMA-Expressing PCa Cells. We have tested the activity of free MMAE and MMAE containing compounds (BFM2, TFM2, and TFM3) against LNCaP (PSMA+) and DU145 (PSMA−) cells. MMAE was very potent against both LNCaP (IC_{50} = 1.06 nM) and DU145 (IC_{50} = 1.08 nM) (Figure 6b). The activity of BFM2, TFM2, and TFM3 on LNCaP (IC_{50} = 4.4 nM, 5.4 nM, and 3.5 nM, respectively) was higher than their activity on DU145 (IC_{50} = 909 nM, 313 nM, and 243 nM, respectively) (Figure 6c−e). This supports the targeting effect of these molecules on the PSMA+ LNCaP cells. We then tested the cytotoxicity of all compounds in the presence of TTR (1 μM). There was no significant effect of TTR on the activity of all compounds toward LNCaP cells (IC_{50} = 2.1 nM, 8.0 nM, and 4.1 nM, for BFM2, TFM2, and TFM3, respectively). In PSMA− DU145 cells, while there was no major effect of TTR on the activity of MMAE (IC_{50} = 0.9 nM) and BFM2 (IC_{50} = 784 nM), there was a 1.7 fold decrease in the activity of TFM2 (IC_{50} = 529 nM) and 3.2-fold decrease in the activity of TFM3 (IC_{50} = 794 nM) when TTR was present. Similar data was observed when we tested our molecules in HeLa cell (PSMA− cells derived from cervical cancer cells (Figure S6). These data support our hypothesis that TTR can indeed sequester (and lower the toxicity) of TFMs toward cells lacking the targeted receptor. Importantly, the more hydrophilic TFM3 has the lowest activity against DU145 (>200-fold lower activity than the activity against LNCaP), which as we hypothesized could be due to the lower passive diffusion across cell membrane. Therefore, we decided to further evaluate the pharmacokinetic properties of TFM3 in rats and its efficacy in mice xenograft tumor models in comparison to BFM2.

TFM3 Is More Stable than BFM2 in Rat and Mouse Serum and Does Not Interfere with Holo-RBP−TTR Interaction. The valine−citrulline linkers are stable in human serum. However, it has been reported that these linkers can be hydrolyzed in mouse serum by extracellular carboxylesterase 1c (Ces1c).[37] Therefore, we assessed the stability of TFM3 and BFM2 in buffer, human, rat, and mouse sera before performing the in vivo pharmacokinetics and efficacy experiments (Figures S7−S9). No significant hydrolysis was observed for TFM3 and BFM2 (100% remaining) in buffer and human serum at 37 °C for at least 24 h. While there was some hydrolysis of the linker in rat serum, the majority of TFM3 (92.1 ± 1.1% and 80.4 ± 0.8% remaining after 12 and 24 h, respectively) and BFM2 (82.1 ± 1.9% and 60.2 ± 1.8% remaining after 12 and 24 h, respectively) were intact. As anticipated, the valine−citrulline linkers of TFM3 and BFM2 exhibited much lower stability in mouse serum (Figure S7d). There was 56.4 ± 1.1% of TFM3 remaining after 12 h and 16.1 ± 0.8% remaining after 24 h (Figure S8d). In contrast, BFM2 lost ∼80% and 100% of the conjugated MMAE after 12 and 24 h, respectively (Figure S9d).

We investigated the effect of TTR on the enhanced stability of TFM3 over BFM2. Our data suggest that only ∼20% protection for TFM3 is provided by TTR. This is expected since the hydrolysis site on the valine−citrulline linker is at least 45 Å away from TTR (previous studies showed that 20 Å is the ideal linker length for maximum protection against peptides hydrolysis).[9] Therefore, we predict that the majority of the stabilizing effect against serum proteases is likely to come from the steric bulk of the TTR binding module.

The main function of TTR is to transport holo-RBP (∼1.5 μM).[38] TTR also acts as a back-up carrier of thyroxine (T_4), however, due to the presence of two other T_4 transport proteins in blood, these T_4 sites remain largely unoccupied in humans (<1% T_4 bound).[39] The holo-RBP binding sites on TTR are positioned orthogonal to the nonoverlapping T_4 binding sites (where TFM3 binds), therefore the binding of holo-RBP to TTR is not affected by the presence or absence of T_4. In an effort to rule out the possibility that the extended linker in TFM3 would interfere with the holo-RBP binding to TTR, we performed a Western Blot assay in human serum (Figure S10). Our results confirmed data reported in literature for T_4, and showed that TTR can indeed interact with both TFM3 and holo-RBP in concert.

TTR Extended Circulation $t_{1/2}$ of TFM3 in Rats. We have evaluated the pharmacokinetic properties of TFM3 and BFM2 (both containing MMAE) in rats. TFM3 (0.16 μmol/kg) and BFM2 (0.32 μmol/kg, twice the dose of TFM3) were administered as single IV doses to jugular vein cannulated male SD rats (Figure 4f). Blood samples were withdrawn from the jugular vein cannula at predetermined time points (ranging from 5 min to 24 h) and concentrations of test compounds were quantitated using a validated LC−MS/MS method (Figure S11). The pharmacokinetic profile of TFM3 was markedly different than BFM2. The concentrations of TFM3 were significantly higher than BFM2 at any given time, despite the administration of twice as much BFM2. While there was no measurable amount of BFM2 after 4 h, TFM3 was still present even after 24 h (Figure 4f). There was ∼5.2 fold increase in the $t_{1/2}$ of TFM3 compared to BFM2 ($t_{1/2}$ = 3.84 ± 0.18 h vs 0.73 ± 0.06 h, respectively). Importantly, the MRT (∼8-fold higher; 4.1 ± 0.68 h for TFM3 and 0.49 ± 0.1 h for BFM2) and AUC (exposure) (∼3-fold higher; 4659 ± 561 nM.h for TFM3 and

DOI: 10.1021/acs.molpharmaceut.9b00432
Mol. Pharmaceutics 2019, 16, 3237−3252

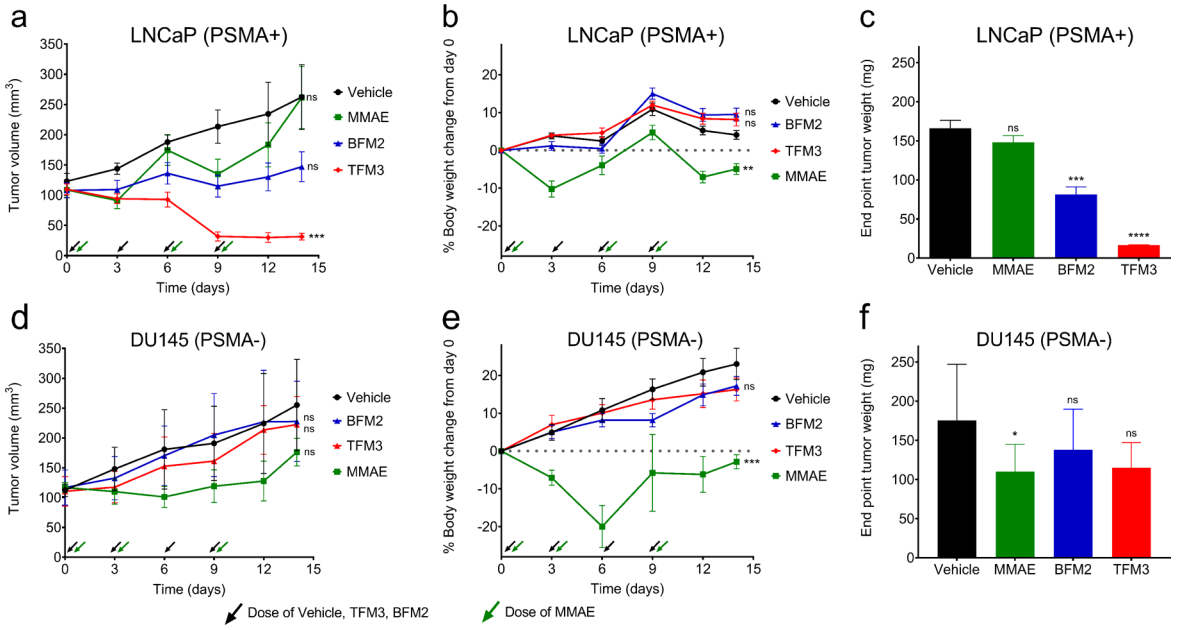

Figure 7. Antitumor efficacy of TFM3 and BFM2 in LNCaP (PSMA+) and DU145 (PSMA−) xenograft mouse models of metastatic PCa. (a) Male athymic nu/nu mice (n = 6) with LNCaP (PSMA+) tumors received TFM3, BFM2, MMAE, or vehicle at a dose of 300 nmol/kg via i.p. injection as indicated by black (for TFM3, BFM2, or vehicle) or green (for MMAE) arrows. Each point represents mean (±s.d.) tumor volume (mm^3). (b) Mean (±s.d.) % body weight changes from the beginning of treatment in the same mice with LNCaP tumors. (c) Mean (±s.d.) weight of excised LNCaP tumors from each treatment group after 14 days. (d) Male athymic nu/nu (n = 6) mice with DU145 (PSMA−) tumors received TFM3, BFM2, MMAE, or vehicle at a dose of 300 nmol/kg via i.p. injection as indicated by black or green arrows. Each point represents mean (±s.d.) tumor volume (mm^3). (e) Mean (±s.d.) % body weight changes from the beginning of treatment in the same mice with DU145 tumors. (f) Mean (±s.d.) weight of excised DU145 tumors from each treatment group after 14 days. The significance of differences was measured by one-way ANOVA followed by Tukey's multiple comparison test (ns, not significant; $*p \leq 0.05$; $**p \leq 0.01$; $***p \leq 0.001$; $****p \leq 0.0001$).

1425 ± 206 nM h for BFM2) were significantly higher for TFM3 than BFM2. This data is consistent with the data obtained for TFM1 and strongly supports and validates our approach that TTR recruitment can indeed enhance the $t_{1/2}$ and pharmacokinetic profile of TFMs in vivo.

TFM3 Has Enhanced Antitumor Activity in Xenograft Mouse Model of Human Metastatic Prostate Cancer. Before performing the efficacy study, we did a preliminary evaluation of the toxicity of TFM3 and BFM2 in mice. Four groups (n = 4 per group) of CD-1 male mice received multiple i.p. doses of TFM3, BFM2, MMAE, or vehicle (300 nmol/kg every 3 days; total four doses) and the body weights of the animals were monitored for 12 days (Figure S12). MMAE served as a control for untargeted cytotoxicity. This dosing regimen is well under the reported maximum tolerated dose for MMAE (between 700 to 1400 nmol/kg)[40] and also reported to be used for a number of ligand targeted MMAE conjugates.[41,42] Two additional groups (n = 4 per group) were also administered higher doses of TFM3 and BFM2 (600 nmol/kg). The toxicity was evaluated by monitoring the body weight of the treated animals. Animals that lost >20% of their weight were euthanized. As expected, there was a major decrease in the body weight of all mice treated with MMAE. Our data showed that both TFM3 and BFM2 were tolerated at the 300 nmol/kg dose. There was a significant ($p \leq 0.001$) drop of the body weight of mice treated with BFM2 at the 600 nmol/kg. From these studies, the 300 nmol/kg dose was selected to investigate the anticancer efficacy of our test compounds.

We then examined the antitumor activity of test compounds in nude mice bearing human LNCaP (PSMA+) and DU145 (PSMA−) prostate tumors (Figure 7). After xenograft tumors reached a volume of 100−150 mm^3, mice were randomized into 4 treatment groups with similar mean tumor volume. Equivalent molar quantities of TFM3, BFM2, MMAE (300 nmol/kg), or saline (vehicle control) were administered (i.p.) every 3 days (total of 4 doses) to four groups of animals (n = 6 per group). Animal weights were measured throughout the study as an indication of toxicity. The antitumor activity of test compounds was evaluated by measuring the change in tumor size over time. Our data showed that TFM3 effectively suppressed tumor growth of the LNCaP cells after the third dose (~70% decrease in tumor volume). The antitumor activity of TFM3 was significantly ($p \leq 0.001$) higher than BFM2, free MMAE, and vehicle (Figure 7a). After this time point, the tumor size in the animals treated with TFM3 did not change significantly up to the end of the studied period (14 days) (Figure 7c). The activity of MMAE was lower than both BFM2 and TFM3. This is expected since MMAE is a lipophilic molecule that has a higher volume of distribution (8400 mL/kg)[43] compared to TFM3 (144 mL/kg), and therefore the effective dose reaching the tumor via untargeted delivery is low. The extensive distribution of MMAE was clear from the dramatic decrease (>10%) in the body weight of animals after the first dose, which necessitated skipping the second dose for the MMAE group (Figure 7b). On the other hand, no significant weight loss or any apparent signs of toxicity were observed for TFM3 and BFM2 treatment groups, and all mice survived the entirety of the in vivo study.

We repeated the same efficacy experiment in the DU145 (PSMA−) tumor model (Figure 7d−f). As expected, the tumor volumes of the TFM3 and BFM2 treatment groups were not significantly different compared to the vehicle treated group (Figure 7d). The BFM2 and TFM3 treated animals did

DOI: 10.1021/acs.molpharmaceut.9b00432
Mol. Pharmaceutics 2019, 16, 3237−3252

not show any sign of toxicities in terms of body weight (Figure 7e). None of the treatment groups, except MMAE ($p \leq 0.05$), showed significant anticancer effects in terms of end point tumor weight (Figure 7f). At the same time, the MMAE treated animals showed significant signs of toxicities, that is, body weight reduction, reduced food and water intake, and difficulties in movement. Because of the signs of severe toxicity, the third dose of MMAE was not administered in DU145 model. Unscheduled euthanasia were carried out for two MMAE treated animals on day nine and 12 during the study due to a reduction of greater than 20% of body weight and moribund symptoms.

Summarizing the results of the efficacy experiments, one can conclude that incorporating the TTR ligand **2** in TFM3 significantly limited the toxicity of MMAE on healthy tissues, and at the same time substantially enhanced the antitumor efficacy of TFM3 compared to BFM2. This indicates that the enhanced tumor uptake of TFM3 in LNCaP (PSMA+) tumors is due to the prolonged blood circulation and exposure (AUC) of TFM3 compared to BFM2, especially since the binding affinity of BFM2 to PSMA in buffer (K_i = 7.2 nM) and its activity on LNCaP (PSMA+) cells (IC_{50} = 2.1 nM) are slightly higher than that for TFM3 (K_i = 16.4 nM and IC_{50} = 4.1 nM).

CONCLUSION

Small-format LTDs have several advantages over traditional nontargeted therapeutic agents. However, the poor pharmacokinetic profile of these molecules remains an important issue that is yet to be resolved. Therefore, strategies that enhance the pharmacokinetic properties of LTDs, while retaining their more effective tumor penetrating properties, could at last make these small-size conjugates a viable alternative to targeted large macromolecules that are disproportionately biased toward hematologic cancers over solid tumors. While much of the effort in this field is focused on maintaining the small size and hydrophilicity of LTDs for efficient and selective penetration into solid tumor tissues, the trade-off is lower overall tumor uptake and lower in vivo efficacy due to rapid systemic clearance.

In this study, we have developed a new concept and platform approach, which combines advantages from both large macromolecules (e.g., extended circulation $t_{1/2}$) and small LTDs (e.g., high tumor penetration and hydrophilicity). Endowing targeted chemotherapeutic agents with the small and hydrophilic TTR ligand **2** allows the generation of hydrophilic small TFMs (<3 kDa) that, in contrast to typical LTDs, have enhanced pharmacokinetic and efficacy profiles. The modular design of the TFMs allows each TFM component to be optimized without dramatically affecting the performance of other modules. The smaller size of TFMs could offer a number of additional advantages such as lower antigenicity, lower production cost, and chemical stability. The promising pharmacokinetics and efficacy suggests that TFM3 may provide a valuable lead for developing next-generation PSMA-targeted LTDs as potential therapeutics for mCRPC, a disease that is currently incurable. To the best of our knowledge, this is the first demonstration of a successful approach that not only extends the circulation $t_{1/2}$ but also maintains the smaller size and the hydrophilicity of targeted anticancer agents containing hydrophobic payloads.

The success of our approach in delivering both hydrophilic Cy7 and hydrophobic MMAE to the intracellular compartment of cancer cells indicates that this approach could be utilized for other small molecules targeting many types of cancers, as well as other diseases. We envision that the new TTR ligands we developed herein to be potentially useful for enhancing the pharmacokinetic properties and hydrophilicity of various biomolecules without significantly increasing their size. This should broaden the scope and utility of our approach.

ASSOCIATED CONTENT

Supporting Information

The Supporting Information is available free of charge on the ACS Publications website at DOI: 10.1021/acs.molpharmaceut.9b00432.

Supporting figures, schemes, and further chemical characterization experiments (PDF)

AUTHOR INFORMATION

Corresponding Author

*E-mail: malhamadsheh@pacific.edu.

ORCID

Mamoun M. Alhamadsheh: 0000-0003-4325-7044

Author Contributions

§A.P. and W.A. contributed equally to this work.

Notes

The authors declare no competing financial interest.

ACKNOWLEDGMENTS

This work was supported by the US National Institutes of Health Grant No. 1R15GM129676-01 (M.M.A.). The support by a National Science Foundation Instrumentation grant (NSF-MRI-0722654) is gratefully acknowledged. Thanks to Andreas Franz, Vyacheslav Samoshin, and Jianhua Ren for NMR and mass spectrometric analysis.

REFERENCES

(1) Srinivasarao, M.; Galliford, C. V.; Low, P. S. Principles in the design of ligand-targeted cancer therapeutics and imaging agents. *Nat. Rev. Drug Discovery* **2015**, *14* (3), 203−19.

(2) Srinivasarao, M.; Low, P. S. Ligand-Targeted Drug Delivery. *Chem. Rev.* **2017**, *117* (19), 12133−12164.

(3) Vlashi, E.; Kelderhouse, L. E.; Sturgis, J. E.; Low, P. S. Effect of folate-targeted nanoparticle size on their rates of penetration into solid tumors. *ACS Nano* **2013**, *7* (10), 8573−82.

(4) Thurber, G. M.; Schmidt, M. M.; Wittrup, K. D. Antibody tumor penetration: transport opposed by systemic and antigen-mediated clearance. *Adv. Drug Delivery Rev.* **2008**, *60* (12), 1421−34.

(5) Waller, K. V.; Ward, K. M.; Mahan, J. D.; Wismatt, D. K. Current concepts in proteinuria. *Clin. Chem.* **1989**, *35* (5), 755−65.

(6) Allen, T. M. Ligand-targeted therapeutics in anticancer therapy. *Nat. Rev. Cancer* **2002**, *2* (10), 750−63.

(7) Umbricht, C. A.; Benešová, M.; Schibli, R.; Müller, C. Preclinical Development of Novel PSMA-Targeting Radioligands: Modulation of Albumin-Binding Properties To Improve Prostate Cancer Therapy. *Mol. Pharmaceutics* **2018**, *15* (6), 2297−2306.

(8) Kelly, J.; Amor-Coarasa, A.; Ponnala, S.; Nikolopoulou, A.; Williams, C.; Schlyer, D.; Zhao, Y.; Kim, D.; Babich, J. W. Trifunctional PSMA-targeting constructs for prostate cancer with unprecedented localization to LNCaP tumors. *Eur. J. Nucl. Med. Mol. Imaging* **2018**, *45* (11), 1841−1851.

(9) Penchala, S. C.; Miller, M. R.; Pal, A.; Dong, J.; Madadi, N. R.; Xie, J.; Joo, H.; Tsai, J.; Batoon, P.; Samoshin, V.; Franz, A.; Cox, T.; Miles, J.; Chan, W. K.; Park, M. S.; Alhamadsheh, M. M. A biomimetic approach for enhancing the in vivo half-life of peptides. *Nat. Chem. Biol.* **2015**, *11* (10), 793−8.

DOI: 10.1021/acs.molpharmaceut.9b00432
Mol. Pharmaceutics 2019, 16, 3237−3252

(10) Penchala, S. C.; Connelly, S.; Wang, Y.; Park, M. S.; Zhao, L.; Baranczak, A.; Rappley, I.; Vogel, H.; Liedtke, M.; Witteles, R. M.; Powers, E. T.; Reixach, N.; Chan, W. K.; Wilson, I. A.; Kelly, J. W.; Graef, I. A.; Alhamadsheh, M. M. AG10 inhibits amyloidogenesis and cellular toxicity of the familial amyloid cardiomyopathy-associated V122I transthyretin. *Proc. Natl. Acad. Sci. U. S. A.* **2013**, *110* (24), 9992−7.
(11) Becke, A. D. Density-functional thermochemistry. III. The role of exact exchange. *J. Chem. Phys.* **1993**, *98* (7), 5648−5652.
(12) McLean, A.; Chandler, G. Contracted Gaussian basis sets for molecular calculations. I. Second row atoms, Z= 11−18. *J. Chem. Phys.* **1980**, *72* (10), 5639−5648.
(13) Krishnan, R.; Binkley, J. S.; Seeger, R.; Pople, J. A. Self-Consistent Molecular Orbital Methods. 20. Basis set for correlated wave-functions. *J. Chem. Phys.* **1980**, *72*, 650−54.
(14) Frisch, M. J.; Trucks, G. W.; Schlegel, H. B.; Scuseria, G. E.; Robb, M. A.; Cheeseman, J. R.; Scalmani, G.; Barone, V.; Mennucci, B.; Petersson, G. A.; Nakatsuji, H.; Caricato, M.; Li, X.; Hratchian, H. P.; Izmaylov, A. F.; Bloino, J.; Zheng, G.; Sonnenberg, J. L.; Hada, M.; Ehara, M.; Toyota, K.; Fukuda, R.; Hasegawa, J.; Ishida, M.; Nakajima, T.; Honda, Y.; Kitao, O.; Nakai, H.; Vreven, T.; Montgomery, J. A., Jr.; Peralta, J. E.; Ogliaro, F.; Bearpark, M.; Heyd, J. J.; Brothers, E.; Kudin, K. N.; Staroverov, V. N.; Kobayashi, R.; Normand, J.; Raghavachari, K.; Rendell, A.; Burant, J. C.; Iyengar, S. S.; Tomasi, J.; Cossi, M.; Rega, N.; Millam, J. M.; Klene, M.; Knox, J. E.; Cross, J. B.; Bakken, V.; Adamo, C.; Jaramillo, J.; Gomperts, R.; Stratmann, R. E.; Yazyev, O.; Austin, A. J.; Cammi, R.; Pomelli, C.; Ochterski, J. W.; Martin, R. L.; Morokuma, K.; Zakrzewski, V. G.; Voth, G. A.; Salvador, P.; Dannenberg, J. J.; Dapprich, S.; Daniels, A. D.; Farkas, O.; Foresman, J. B.; Ortiz, J. V.; Cioslowski, J.; Fox, D. J. *Gaussian 09*; Gaussian, Inc.: Wallingford, CT, 2009.
(15) Lang, P. T.; Brozell, S. R.; Mukherjee, S.; Pettersen, E. F.; Meng, E. C.; Thomas, V.; Rizzo, R. C.; Case, D. A.; James, T. L.; Kuntz, I. D. DOCK 6: Combining techniques to model RNA−small molecule complexes. *RNA* **2009**, *15* (6), 1219−1230.
(16) Zhang, A. X.; Murelli, R. P.; Barinka, C.; Michel, J.; Cocleaza, A.; Jorgensen, W. L.; Lubkowski, J.; Spiegel, D. A. A remote arene-binding site on prostate specific membrane antigen revealed by antibody-recruiting small molecules. *J. Am. Chem. Soc.* **2010**, *132* (36), 12711−6.
(17) Pettersen, E. F.; Goddard, T. D.; Huang, C. C.; Couch, G. S.; Greenblatt, D. M.; Meng, E. C.; Ferrin, T. E. UCSF Chimera–a visualization system for exploratory research and analysis. *J. Comput. Chem.* **2004**, *25* (13), 1605−12.
(18) Alhamadsheh, M. M.; Connelly, S.; Cho, A.; Reixach, N.; Powers, E. T.; Pan, D. W.; Wilson, I. A.; Kelly, J. W.; Graef, I. A. Potent kinetic stabilizers that prevent transthyretin-mediated cardiomyocyte proteotoxicity. *Sci. Transl. Med.* **2011**, *3* (97), 97ra81.
(19) Choi, S.; Connelly, S.; Reixach, N.; Wilson, I. A.; Kelly, J. W. Chemoselective small molecules that covalently modify one lysine in a non-enzyme protein in plasma. *Nat. Chem. Biol.* **2010**, *6* (2), 133−9.
(20) Choi, S.; Kelly, J. W. A competition assay to identify amyloidogenesis inhibitors by monitoring the fluorescence emitted by the covalent attachment of a stilbene derivative to transthyretin. *Bioorg. Med. Chem.* **2011**, *19* (4), 1505−14.
(21) Chang, S. S.; O'Keefe, D. S.; Bacich, D. J.; Reuter, V. E.; Heston, W. D.; Gaudin, P. B. Prostate-specific membrane antigen is produced in tumor-associated neovasculature. *Clin. Cancer Res.* **1999**, *5* (10), 2674−81.
(22) Silver, D. A.; Pellicer, I.; Fair, W. R.; Heston, W. D.; Cordon-Cardo, C. Prostate-specific membrane antigen expression in normal and malignant human tissues. *Clin. Cancer Res.* **1997**, *3* (1), 81−5.
(23) Haberkorn, U.; Eder, M.; Kopka, K.; Babich, J. W.; Eisenhut, M. New Strategies in Prostate Cancer: Prostate-Specific Membrane Antigen (PSMA) Ligands for Diagnosis and Therapy. *Clin. Cancer Res.* **2016**, *22* (1), 9−15.
(24) Eiber, M.; Fendler, W. P.; Rowe, S. P.; Calais, J.; Hofman, M. S.; Maurer, T.; Schwarzenboeck, S. M.; Kratowchil, C.; Herrmann, K.; Giesel, F. L. Prostate-Specific Membrane Antigen Ligands for Imaging and Therapy. *J. Nucl. Med.* **2017**, *58* (Suppl 2), 67S−76S.
(25) Hadaschik, B. A.; Boegemann, M. Why Targeting of PSMA Is a Valuable Addition to the Management of Castration-Resistant Prostate Cancer: The Urologist's Point of View. *J. Nucl. Med.* **2017**, *58* (8), 1207−1209.
(26) Francisco, J. A.; Cerveny, C. G.; Meyer, D. L.; Mixan, B. J.; Klussman, K.; Chace, D. F.; Rejniak, S. X.; Gordon, K. A.; DeBlanc, R.; Toki, B. E.; Law, C. L.; Doronina, S. O.; Siegall, C. B.; Senter, P. D.; Wahl, A. F. cAC10-vcMMAE, an anti-CD30-monomethyl auristatin E conjugate with potent and selective antitumor activity. *Blood* **2003**, *102* (4), 1458−65.
(27) Gordon, M. R.; Canakci, M.; Li, L.; Zhuang, J.; Osborne, B.; Thayumanavan, S. Field Guide to Challenges and Opportunities in Antibody-Drug Conjugates for Chemists. *Bioconjugate Chem.* **2015**, *26* (11), 2198−215.
(28) Kozikowski, A. P.; Zhang, J.; Nan, F.; Petukhov, P. A.; Grajkowska, E.; Wroblewski, J. T.; Yamamoto, T.; Bzdega, T.; Wroblewska, B.; Neale, J. H. Synthesis of urea-based inhibitors as active site probes of glutamate carboxypeptidase II: efficacy as analgesic agents. *J. Med. Chem.* **2004**, *47* (7), 1729−38.
(29) Kularatne, S. A.; Wang, K.; Santhapuram, H. K.; Low, P. S. Prostate-specific membrane antigen targeted imaging and therapy of prostate cancer using a PSMA inhibitor as a homing ligand. *Mol. Pharmaceutics* **2009**, *6* (3), 780−9.
(30) Bulawa, C. E.; Connelly, S.; Devit, M.; Wang, L.; Weigel, C.; Fleming, J. A.; Packman, J.; Powers, E. T.; Wiseman, R. L.; Foss, T. R.; Wilson, I. A.; Kelly, J. W.; Labaudinière, R. Tafamidis, a potent and selective transthyretin kinetic stabilizer that inhibits the amyloid cascade. *Proc. Natl. Acad. Sci. U. S. A.* **2012**, *109* (24), 9629−34.
(31) Bleiberg-Daniel, F.; Le Moullac, B.; Maire, J. C.; Wade, S. Failure of tryptophan deficiency to reduce specifically serum levels of transthyretin or albumin in rats. *J. Nutr.* **1990**, *120* (12), 1610−6.
(32) Vranckx, R.; Savu, L.; Maya, M.; Rouaze-Romet, M.; Nunez, E. A. Immunological quantitation of rat and mouse thyroxine-binding globulins. Ontogenesis and sex-dependence of the circulating levels of the thyroxine-binding globulins. *Eur. J. Endocrinol.* **1990**, *123* (6), 649−56.
(33) Schreiber, G. The evolutionary and integrative roles of transthyretin in thyroid hormone homeostasis. *J. Endocrinol.* **2002**, *175* (1), 61−73.
(34) Episkopou, V.; Maeda, S.; Nishiguchi, S.; Shimada, K.; Gaitanaris, G. A.; Gottesman, M. E.; Robertson, E. J. Disruption of the transthyretin gene results in mice with depressed levels of plasma retinol and thyroid hormone. *Proc. Natl. Acad. Sci. U. S. A.* **1993**, *90* (6), 2375−9.
(35) Wang, X.; Ma, D.; Olson, W. C.; Heston, W. D. In vitro and in vivo responses of advanced prostate tumors to PSMA ADC, an auristatin-conjugated antibody to prostate-specific membrane antigen. *Mol. Cancer Ther.* **2011**, *10* (9), 1728−39.
(36) Taylor, R. M.; Severns, V.; Brown, D. C.; Bisoffi, M.; Sillerud, L. O. Prostate cancer targeting motifs: expression of αv $\beta 3$, neurotensin receptor 1, prostate specific membrane antigen, and prostate stem cell antigen in human prostate cancer cell lines and xenografts. *Prostate* **2012**, *72* (5), 523−32.
(37) Dorywalska, M.; Dushin, R.; Moine, L.; Farias, S. E.; Zhou, D.; Navaratnam, T.; Lui, V.; Hasa-Moreno, A.; Casas, M. G.; Tran, T. T.; Delaria, K.; Liu, S. H.; Foletti, D.; O'Donnell, C. J.; Pons, J.; Shelton, D. L.; Rajpal, A.; Strop, P. Molecular Basis of Valine-Citrulline-PABC Linker Instability in Site-Specific ADCs and Its Mitigation by Linker Design. *Mol. Cancer Ther.* **2016**, *15* (5), 958−70.
(38) Ingenbleek, Y.; Young, V. Transthyretin (prealbumin) in health and disease: nutritional implications. *Annu. Rev. Nutr.* **1994**, *14*, 495−533.
(39) Johnson, S. M.; Wiseman, R. L.; Sekijima, Y.; Green, N. S.; Adamski-Werner, S. L.; Kelly, J. W. Native state kinetic stabilization as a strategy to ameliorate protein misfolding diseases: a focus on the transthyretin amyloidoses. *Acc. Chem. Res.* **2005**, *38* (12), 911−21.

DOI: 10.1021/acs.molpharmaceut.9b00432
Mol. Pharmaceutics 2019, 16, 3237−3252

(40) Crisp, J. L.; Savariar, E. N.; Glasgow, H. L.; Ellies, L. G.; Whitney, M. A.; Tsien, R. Y. Dual targeting of integrin $\alpha v\beta 3$ and matrix metalloproteinase-2 for optical imaging of tumors and chemotherapeutic delivery. *Mol. Cancer Ther.* **2014**, *13* (6), 1514−25.
(41) Buckel, L.; Savariar, E. N.; Crisp, J. L.; Jones, K. A.; Hicks, A. M.; Scanderbeg, D. J.; Nguyen, Q. T.; Sicklick, J. K.; Lowy, A. M.; Tsien, R. Y.; Advani, S. J. Tumor radiosensitization by monomethyl auristatin E: mechanism of action and targeted delivery. *Cancer Res.* **2015**, *75* (7), 1376−1387.
(42) Liu, Y.; Bajjuri, K. M.; Liu, C.; Sinha, S. C. Targeting cell surface alpha(v)beta(3) integrin increases therapeutic efficacies of a legumain protease-activated auristatin prodrug. *Mol. Pharmaceutics* **2012**, *9* (1), 168−75.
(43) Chen, Y.; Samineni, D.; Mukadam, S.; Wong, H.; Shen, B. Q.; Lu, D.; Girish, S.; Hop, C.; Jin, J. Y.; Li, C. Physiologically based pharmacokinetic modeling as a tool to predict drug interactions for antibody-drug conjugates. *Clin. Pharmacokinet.* **2015**, *54* (1), 81−93.

DOI: 10.1021/acs.molpharmaceut.9b00432
Mol. Pharmaceutics 2019, 16, 3237−3252